MAXIMIZING SPECIFIC WORK OUTPUT EXTRACTED FROM ENGINE EXHAUST WITH NOVEL INVERTED BRAYTON CYCLES OVER A LARGE RANGE OF OPERATING CONDITIONS

Noémie **Chagnon-Lessard**[1], Colin **Copeland**[2], François **Mathieu-Potvin**[*1], Louis **Gosselin**[1]

(**bold** font weight for family name)

[1] *Department of Mechanical Engineering, 1065, Avenue de la Médecine, Université Laval, Quebec City, Quebec, Canada, G1V 0A6*

[2] *Powertrain and Vehicle Research Centre, University of Bath, Claverton Down, Bath, BA2 7AY, United Kingdom*

Abstract

The thermal energy contained in internal combustion engine exhaust gases can be converted into mechanical energy by using an Inverted Brayton Cycle (IBC). In this paper, five different versions of the IBC are numerically modeled and optimized to maximize their specific work output. These cycles are: (i) basic IBC, (ii) IBC with liquid water drainage (IBC/D), (iii) IBC with liquid water drainage and a steam turbine (IBC/D/S), (iv) IBC with liquid water drainage and a refrigeration cycle (IBC/D/R), and (v) IBC with liquid water drainage, a steam turbine and a refrigeration cycle (IBC/D/S/R). Among these five systems, three are presented for the first time in the literature (i.e., the IBC/D/S, IBC/D/R and IBC/D/S/R). The optimization runs are performed for a wide range of inlet gases temperatures (from 600 to 1200 K) and heat sink temperatures (from 280 to 340 K), and the results are reported as design charts that provide guidelines for the design of optimal IBC engine heat recovery systems. Among the five IBCs, the IBC/D/S/R has the highest specific work output for the whole range of operating temperatures. A comparison with the subcritical Rankine cycle and Organic Rankine Cycles using isobutane and benzene shows that an IBC system might be a better choice for specific operating temperatures. Liquid water addition in the IBC/D/S/R leads to

[*] Corresponding author.
Email address: Francois.Mathieu-Potvin@gmc.ulaval.ca (F. Mathieu-Potvin).

optimized designs using only the steam turbine at high inlet gas temperatures, indicating that a Rankine cycle is better suited for these conditions.

Keywords: Engine exhaust heat recovery; Inverted Brayton Cycle (IBC); Open Rankine cycle; Bottoming cycles; Water drainage; Design optimization.

Nomenclature

Variables

c_p	specific heat, kJ kg^{-1} K^{-1}
h	enthalpy, kJ kg^{-1}
h_f^o	enthalpy of formation, kJ kg^{-1}
M	molar mass, g mol^{-1}
mf	mass fraction
N	number of moles, mol
P	pressure, kPa
q	specific heat transfer rate, kJ kg^{-1}
R	gas constant, kJ kg^{-1} K^{-1}
s	entropy, kJ kg^{-1} K^{-1}
s_f^o	entropy of formation, kJ kg^{-1} K^{-1}
sh	specific humidity
T	temperature, K
U_R	refrigeration utilization rate
w	specific work output, kJ kg^{-1}
x	vapor quality
y	molar fraction

Greek symbols

ε	heat exchanger effectiveness
η	efficiency

Subscripts

atm	atmospheric
f, g	saturated liquid and saturated gas states
i	species
in	inlet
j	increment, iteration number
liq	liquid state
max	maximum
min	minimum
opt	optimal
out	outlet
pp	pinch point
ref	reference
s	isentropic
sat	saturated
sw	supplied liquid water
tol	tolerance
tot	total
vap	vapor state
w	working fluid

Abbreviations

CO	condenser
CP	compressor
D	related to drainage
EC	economizer
EV	evaporator
GT	gas turbine

IBC	Inverted Brayton Cycle
IC	internal combustion
ORC	Organic Rankine Cycle
PP	pump
R	related to refrigeration cycle
S	related to open Rankine cycle
SH	superheater
ST	steam turbine
VA	valve

1. Introduction

Whether for economic reasons or to mitigate global warming, reducing engine fuel consumption is imperative. In internal combustion (IC) engines, approximately 30% of the energy of combustion is lost in exhaust gases [1]. A way to improve their overall energy conversion efficiency is to add a system capable of recovering the waste heat exiting the engine. Although waste heat can also be recovered from other sources, the exhaust gases contain the largest recovery potential [2], and therefore, several waste heat recovery (WHR) technologies for flue gases have been proposed and investigated. Among the most studied WHR systems for engines are thermodynamic cycles used as bottoming cycles. The Brayton air cycle is one the simplest and cost-effective systems [3]. Nevertheless, Organic Rankine cycles (ORC) are presently considered as one of the most promising WHR technologies for their applicability to both high and low-temperature heat sources [4].

A potential bottoming cycle for IC engines that has recently received a lot of attention is the Inverted Brayton Cycle (IBC). Proposed by Wilson [5], it consists in a simple modification to the Brayton Cycle: the exhaust gases expand to a sub-atmospheric pressure, are cooled, and finally compressed to atmospheric pressure. IBC as a bottoming cycle has other applications than engine heat recovery: gas turbine repowering [6], reheat gas turbine [7], low-temperature cogeneration applications [8], microgas turbine [9], etc.

Among the advantages of IBC over other cycles are its simplicity and the availability of the required turbomachinery components. Lower overall efficiency and fouling/corrosion issues are the most commonly mentioned drawbacks of IBCs when compared to other technologies, which constitute the challenges currently driving the research efforts related to IBCs. One of the first techno-economic studies of an IBC as an engine heat recovery system was done by Bailey [10], where the IBC was referred to as a sub-atmospheric Brayton system. Although the efficiency of the IBC was better than that of pressurized Brayton systems (in which the exhaust provides heat through a heat exchanger to another air stream used as the working fluid), the later was preferred based on cost and potential fouling/corrosion considerations. In 2001, Fujii et al. [11] developed an IBC test rig to demonstrate the concept and measured thermal efficiency values of the order of

1%. This relatively poor performance was due to the low turbine efficiency (~50%), since the turbine had been designed to operate at a larger flow rate than the one used in the test rig.

Selecting the best bottoming cycle for a given application can be quite challenging, which brings to light the need for cycle comparison studies. An influential study by Bianchi and De Pascale [12] compared three bottoming cycles (ORC, Stirling and IBC) for a fixed cold source temperature of 15°C and variable hot source temperatures. In their studies, the ORC offered a specific energy output between 10 and 200 kJ/kg depending on the choice working fluid and available temperature, whereas the specific energy output of the IBC was in the range 10-70 kJ/kg depending on temperature and condensed water mass fraction. They conclude that "the innovative and not yet developed IBC system is a promising solution but not as performing as the ORC technology, especially in the field of very low temperatures (200–400°C). If instead heat fluxes are available at temperature values above 350–400°C, the IBC technology becomes more interesting in terms of achievable efficiency".

Despite its observed efficiency often lower than that of ORC, the interest for IBC has continued to grow. Identifying the contexts in which IBCs can be an adequate solution is still an open question and thus, IBCs have been tested in different applications over the last few years. For example, Chen et al. [1] simulated the performance of IBCs when it is coupled with a light-duty automotive engine operating in a real-world driving cycle where the exhaust flow rate varies in time. A reduction of fuel consumption of 3.15% was calculated when the turbine pressure ratio is constantly optimized. Copeland and Chen [13] also showed that IBC is a promising alternative to turbocompounding.

Additionally, another objective of current research on bottoming cycles is to propose improvements or modifications to IBCs that would increase their overall efficiency to a level that would make them more competitive. For example, Fujii et al. [11] proposed an intercooled inverted Brayton cycle or mirror gas turbine concept to improve performance. Kennedy et al. [14] studied the effect of removing condensed water in the exhaust before the compressor. The benefit of this

modification is the mass flow rate reduction during gases compression, which improves the overall cycle efficiency.

The present study further develops this idea by proposing two new additional modifications to the IBC and evaluating the associated change of performance. The first modification uses the drained water to perform an open Rankine cycle, where the exhaust gases at the gas turbine outlet heats the water before entering a steam turbine. The second one is the addition of a refrigeration cycle upstream of the separation to increase liquid water formation and obtain a colder temperature at compressor inlet. No report of IBC optimization for different combinations of temperature conditions (hot and cold sources) was found; hence its most suited applications remain partly unknown compared to other cycles. Five variations of the IBC are investigated, three of which being new proposed cycles. The main goals of the work are to establish new charts that provide guidelines for optimal designs of IBCs and to compare the performance of the IBC variants with that offered by Rankine cycle and Organic Rankine Cycles. The analysis presented in this paper covers a large set of operating conditions, i.e., an exhaust temperature from 600 to 1200 K, and a coolant temperature from 280 to 340 K. The objective function to maximize is the specific work output w [kJ/kg].

The paper is structured as follows: Section 2 describes the IBCs and the methodology used to perform the numerical simulations; Section 3 explains the modeling method used for each piece of equipment; Section 4 describes the optimization problems; Section 5 presents the results of the optimization runs by means of design charts; and in Section 6, examples of applications are provided.

2. Problem statement

The systems considered in this paper include two cycles that have already been presented in literature [1] [14]: (i) the basic Inverted Brayton Cycle (IBC) and (ii) the IBC with liquid water drainage (IBC/D). Moreover, three novel cycles are presented in this paper: (iii) the IBC/D with a

steam turbine (IBC/D/S), (iv) the IBC/D with a refrigeration cycle (IBC/D/R), and (v) the IBC/D with a steam turbine and a refrigeration cycle (IBC/D/S/R).

2.1. Inverted Brayton Cycle (IBC)

The Inverted Brayton Cycle is an open cycle built with three main components: an expander, a heat exchanger, and a compressor. The architecture and thermodynamic diagram of the IBC are given in Fig. 1. The exhaust gases exiting the engine enter the IBC at state {1} at atmospheric pressure, expand in the gas turbine (GT) and leave at state {2}. The heat exchanger cools down the gases to state {3} by transferring the heat to a coolant at constant pressure. Part of the water contained in the gases being condensed in some cases, this heat exchanger will be referred to as the condenser (CO) for the rest of the paper. The gas stream is compressed back to atmospheric pressure where it leaves the compressor (CP) at state {4}.

The fuel used in the upper cycle (engine) is considered to have a hydrogen to carbon ratio equal to 2, and an oxygen to carbon ratio of zero, as for typical hydrocarbon fuels. Assuming a specific humidity of 0.01, the equation for complete combustion considering no excess air is [14]:

$$\begin{aligned} &CH_2 + \frac{3}{2}O_2 + \frac{39}{7}N_2 + \frac{3}{42}Ar + 0.115H_2O \\ &\rightarrow CO_2 + \frac{39}{7}N_2 + \frac{3}{42}Ar + 0.615H_2O \end{aligned} \tag{1}$$

It is now possible to calculate molar and mass fractions of each species in the exhaust gases. For enthalpy and entropy calculations, the specific heat is determined with the following correlation for ideal gases:

$$\overline{c}_{p,i} = M_i c_{p,i} = M_i \left(a_i + b_i T + c_i T^2 + d_i T^3 \right) \tag{2}$$

where $\overline{c}_p$ is the molar specific heat, M the molar mass, c_p the mass specific heat, and a_i to d_i coefficients specific to each species i (see table A.2c of [15]). Eq. (2) is used for CO_2, N_2, and vapor H_2O. Ar has a c_p value independent of temperature.

2.2. Inverted Brayton Cycle with liquid water drainage (IBC/D)

When the gas stream is sufficiently cooled down, condensation occurs in the condenser, and a part of the total water content can be drained before entering the compressor (see Fig. 2a). The advantage of this modification is the flow rate reduction in the compressor, leading to a reduced work input for certain conditions. Fig. 2b follows the thermodynamic states of the exhaust gases (including water vapor), while Fig. 2c shows the water only (liquid and vapor). The exhaust gaseous part undergoes the same evolution as in the IBC, and the liquid water is separated from the gases after state {3} to reach state {6} (or state $\{3_{liq}\}$). It should be noted that the pressure of states {1}, {2}, {4} (or state $\{3_{vap}\}$) and {5} in Fig. 2c are the water partial pressure (vapor pressure). State {6} (state $\{3_{liq}\}$) is compressed liquid water at the lowest pressure of the exhaust gases (at states {2}, {3} and {4} in Fig. 2b) represented by the line P_2 in Fig. 2c. A pump (PP) brings the liquid water to atmospheric pressure at state {7}.

The liquid mass fraction at state {3} is found by first calculating the vapor mass fraction. Since the pressure ratio is equal to the molar fraction for ideal gases, the vapor pressure P_{vap} is:

$$P_{vap} = P_{tot}\left(N_{H_2O}/N_{tot}\right) \tag{3}$$

When $P_{vap} > P_{sat}$, the water content at state {3} is larger than what the gas mixture can hold. Thus, a fraction of the water has condensed and can be removed before entering the compressor. The Arden Buck equation for $T > 0$ °C, which is a modified version of the one presented in [16], is used to calculate P_{sat}:

$$P_{sat}(T) = 0.61121\exp\left[\left(18.678 - \frac{T}{234.5}\right)\left(\frac{T}{257.14+T}\right)\right] \tag{4}$$

The vapor molar fraction in the mixture is found with Eq. (5), and the vapor and liquid mass fractions are determined with Eq. (6)

$$y_{H_2O,vap} = P_{sat}/P \tag{5}$$

$$
\begin{aligned}
mf_{H_2O,vap} &= y_{H_2O,vap} N_{dry} M_{H_2O} \\
mf_{H_2O,liq} &= mf_{H_2O} - mf_{H_2O,vap} \\
N_{dry} &= \frac{N_{CO_2} + N_{N_2} + N_{Ar}}{1 - y_{H_2O,vap}}
\end{aligned}
\tag{6}
$$

where N_{dry} is the number of moles of the species in the mixture apart from water. Eqs. (3), (5) and (6) are taken from Chapter 14 of [15].

2.3. Inverted Brayton Cycle with liquid water drainage and steam turbine (IBC/D/S)

Figure 3 shows the IBC/D/S, the first novel cycle proposed in this paper. It consists of an IBC with liquid water drainage, where the drained liquid water (state {7} or $\{4_{liq}\}$ in Fig. 3c) flows in an open Rankine cycle to produce work in a steam turbine. More specifically, the condensate is first compressed to state {8} with a pump (PP1 in Fig. 3a) and goes through a heat exchanger (EV/S) to receive heat from the exhaust gases at constant pressure and reach a superheated state (state {9}). The vapor is then expended in a steam turbine (ST) and leaves it at state {10}. In order to lower state {10} pressure below atmospheric pressure and produce more work, a condenser (CO/S) brings the water to the saturated liquid state {11} and a second pump (PP2) takes it to atmospheric pressure at state {12}. The achievable pressure at the steam turbine outlet depends on coolant temperature T_A. Solely subcritical open Rankine cycles are considered here.

As for the exhaust gases, their cooling is partly done in the evaporator EV/S and they enter the CO at state {3}. They leave it at state {4}, liquid water is separated to obtain state {5} (and state $\{4_{vap}\}$ for water), and they are put back to atmospheric pressure at state {6} in the CP. Noticeably, this cycle can only work if there is liquid water formed at state {4} and if pressure and temperature of state {9} are high enough to produce work in the ST. In the model, it was assumed that when the last requirement is not met, the right cycle to use is the IBC/D and that when both requirements are not satisfied, the IBC is the cycle to use.

As this cycle is proposed for the first time in literature, Table A.1 describes the IBC/D/S thermodynamic states using the optimized design for a specific case of T_1 and T_A.

2.4. Inverted Brayton Cycle with liquid water drainage and refrigeration cycle (IBC/D/R)

The lower the temperature of a fluid at a compressor inlet, the smaller the work needed to reach the compressor outlet pressure. Thus, a refrigeration cycle could be used to cool the gases before the compressor. A lower temperature before the compressor may also increase the condensate, which reduces the mass flow rate and thus, the work input.

A vapor-compression cycle is therefore added to the IBC/D just before the drainage, see Fig. 4a. As in the IBC/D, the gas stream is expanded in the GT until state {2} and is cooled down in the CO to state {3} (see Fig. 4b). The refrigerant cools it to state {4} in the evaporator (EV/R), reaching a temperature that depends on the extent to which the refrigeration cycle is used, between T_3 and 273.2 K, corresponding to a 'refrigeration utilization rate' of 0% to 100%, respectively. The separated liquid water (states {7} and $\{4_{liq}\}$, see Fig. 4c) and the gaseous part (states {5} and $\{4_{vap}\}$) are brought back to atmospheric pressure by the PP to state {8}, and the CP to state {6}, respectively.

The refrigerant undergoes a basic vapor-compression cycle. It is evaporated at constant pressure in the evaporator (EV/R) to reach state {a} (see Fig. 4d) that has a temperature 3 K higher than the saturated state to ensure it is superheated. The vapor is compressed by a compressor (CP/R) to state {b}, and then it is condensed to saturated liquid (state {c}) at constant pressure in a condenser (CO/R). Finally, the refrigerant goes through an isenthalpic valve to reach state {d} and returns in the EV/R. The fluid employed in this work is R134a, which is one of the best fluids in the conditions considered here[17].

Again, the IBC/D/R being a new cycle, Table A.2 describes its optimized design thermodynamic states for a specific case of T_1 and T_A.

2.5. Inverted Brayton Cycle with liquid water drainage, steam turbine and refrigeration cycle (IBC/D/S/R)

The last novel cycle is the IBC/D/S/R, which consists of an IBC with liquid water drainage, an open Rankine cycle and a refrigeration cycle, as shown in Fig. 5a. This cycle increases the liquid

water production to a flow rate that would not be possible in the IBC/D/S, thus developing greater power in the steam turbine. Now, the exhaust gases are cooled down by three heat exchangers. The first one (EV/S) uses the hotter part of the exhaust gases after the GT to evaporate the water before the ST, leaving the gaseous mixture at state {3} (see Fig 5b). The second heat exchanger CO brings the exhaust gases to state {4}, at a temperature near that of the coolant. Finally, the third heat exchanger EV/R cools the gases to state {5} at a temperature between T_4 and 273.2 K. The refrigeration cycle is the same as the one in the IBC/D/R (see Fig. 5d) using R134a. The gaseous part at state {6} (and state $\{5_{vap}\}$) is compressed to state {7} and the liquid water at state {8} (state $\{5_{liq}\}$) undergoes the same open Rankine cycle than in the IBC/D/S (see Fig. 5c) leaving the system at state {13}. It should be noted that the pressure P_2 is lower in Fig. 5c than in Fig. 3c because the refrigeration cycle helps reaching lower condensing temperatures. Incidentally, the outlet pressure of the ST is below P_2 in Fig. 3c and above P_2 in Fig. 5c. Figures 1 to 5 are not to the scale.

An example of IBC/D/S/R thermodynamic states is detailed in Table A.3.

2.6. Numerical simulations

The modeling and numerical simulations in this project are performed with in-house MATLAB® scripts [18]. The open-source thermophysical property library CoolProp [19] [20] was used to evaluate thermodynamic properties of water and R134.

The present numerical model has been validated by comparing the results with those obtained by two other authors. Considering an inlet exhaust gases temperature T_1 of 1140 K, a coolant temperature T_A of 293 K, a turbine expansion ratio of ~1.72 ($P_2 = 59$ kPa), and turbine and compressor isentropic efficiencies of ~0.53 and ~0.69 respectively, the experiment of Fujii et al. [11] led to an IBC specific work output of ~12.3 kJ/kg (uncertainty analysis was not provided for the experimental measurement). Using the same parameters, the model gives a specific work output of 11.5 kJ/kg, corresponding to a 6.5% relative difference. With $T_1 = 500°C$, $T_A = 15°C$ and a turbomachinery polytropic efficiency value of 0.8, Figs. 7a and 10a in the simulations of Bianchi and De Pascale [12] show specific work outputs of 25 kJ/kg for the IBC ($P_2 = 30$ kPa), and 35 kJ/kg

for the IBC/D ($P_2 = 40$ kPa, $X_{H_2O,in} = 0.1$). The present model gives 24.7 kJ/kg (IBC) and 33.9 kJ/kg (IBC/D) respectively, i.e. relative difference of 1.2% and 3.2%. Therefore, the agreement between the present model and results from literature can be qualified of good.

3. Equipment modeling methodology

This section explains the modeling of the gas turbine, condenser, compressor, steam turbine, and other heat exchangers. Steady-state is considered, and pressure and heat losses are neglected.

3.1. Gas turbine

The water content stays completely in vapor state for the entire expansion, for all external conditions considered in this paper. The specific work produced by the gas turbine may be expressed by the enthalpy difference between states {1} and {2}, or the isentropic enthalpy evolution multiplied by the gas turbine efficiency:

$$w_{GT} = h_1 - h_2 = \eta_{GT}(h_1 - h_{2s}) \tag{7}$$

By virtue of the Gibbs-Dalton Law for ideal gases [21], the isentropic enthalpy difference can be found for each component and then added together considering their mass fraction mf_i. Each individual enthalpy difference is calculated with the specific heat correlation of Eq. (2):

$$\begin{aligned} h_{1,i} - h_{2s,i} &= \int_{T_{2s}}^{T_1} c_{p,i}(T)dT \\ &= a_i(T_1 - T_{2s}) + \frac{b_i}{2}(T_1^2 - T_{2s}^2) + \frac{c_i}{3}(T_1^3 - T_{2s}^3) + \frac{d_i}{4}(T_1^4 - T_{2s}^4) \\ &= \Delta h_i(T_1, T_{2s}) \end{aligned} \tag{8}$$

Temperature T_1 is a known parameter and finding T_{2s} requires calculating entropy variations. According to Gibbs' relation for a closed and reversible system, and assuming an ideal gas, one finds

$$\Delta s = s_2^\circ - s_1^\circ - R\ln\left(P_2/P_1\right) = 0 \tag{9}$$

where initial and final pressures are known. The procedure to estimate the absolute entropy variation $\left(s_2^{\circ} - s_1^{\circ}\right)$ is similar to that used above for the enthalpy variation. $\left(s_2^{\circ} - s_1^{\circ}\right)$ depends only on T_1 and T_{2s}, and can be calculated by summing the absolute entropy variation of each species:

$$\begin{aligned} s_{2,i}^{\circ} - s_{1,i}^{\circ} &= \int_{T_1}^{T_{2s}} \frac{c_{p,i}(T)}{T} dT \\ &= a_i \ln \frac{T_{2s}}{T_1} + b_i (T_{2s} - T_1) + \frac{c_i}{2}(T_{2s}^2 - T_1^2) + \frac{d_i}{3}(T_{2s}^3 - T_1^3) \\ &= \Delta s_i (T_{2s}, T_1) \end{aligned} \tag{10}$$

weighted by their mass fraction mf_i. When inserting Eq. (10) in Eq. (9), it can be observed that the value of T_{2s} is the only unknown in Eq. (9), and it can be found by using the bisection iterative method [22].

Finally, once the value of T_{2s} is found, Eqs. (7) and (8) can be used to calculate w_{GT}. However, the real final temperature T_2 is needed for other calculations in the cycle. The bisection iterative method is used once again to find T_2 knowing that

$$w_{GT} = h_1 - h_2 = \sum_i mf_i \Delta h_i (T_1, T_2) \tag{11}$$

Eqs. (7) and (9) are taken from Chapters 9 and 12 of [15].

3.2. Condenser

To calculate the state at the condenser outlet (state {3} for IBC/D), the formation of liquid water must be taken into account. The heat transferred to the coolant is expressed by:

$$q = \varepsilon_{CO} q_{\max} \tag{12}$$

where ε_{CO} is the condenser effectiveness, and $q_{\max}$, the maximum heat transfer rate that could be exchanged in the condenser. $q_{\max}$ is determined by the limiting fluid in the heat exchanger. In the context of the paper, the limiting side is the gas stream since the coolant can be chosen and its mass flow rate ratio can be as high as desired. With the hypothetical state {3'} where the mixture reaches the minimum theoretical temperature T_A, the maximum potential heat transfer rate is:

$$q_{\max} = h_2 - h_{3'} = \sum_i mf_i \left(h_{2,i} - h_{3',i} \right) \tag{13}$$

Eq. (8) is used for CO_2, N_2, and H_2O_{vap}, while Ar has a constant c_p and the liquid water enthalpy can be found in thermodynamic tables or specialized software (Section 2.6). Due to the fact that the mass fractions change in the process, the enthalpy of formation (at $T_{ref} = 298$ K) of liquid and vapor water need to be used:

$$\begin{aligned} q_{\max} = & \sum_{i=CO_2,N_2} mf_i \Delta h_i \left(T_2, T_A \right) + mf_{Ar} c_p (T_2 - T_A) \\ & + mf_{in,vap} \left(h^{\circ}_{f,vap} + \Delta h_{vap}(T_2, T_{ref}) \right) \\ & - mf_{out,vap} \left(h^{\circ}_{f,vap} + \Delta h_{vap}(T_A, T_{ref}) \right) \\ & - mf_{out,liq} \left(h^{\circ}_{f,liq} + h(T_A, P_2) - h(T_{ref}, P_{atm}) \right) \end{aligned} \tag{14}$$

Water mass fractions at condenser input and output are calculated with Eqs. (3) to (6), where the vapor pressure P_{vap} has to be greater than the saturation pressure P_{sat} so that the water may condense. The exhaust stream temperature at the condenser output T_3 is found with the iterative bisection method by equating the real heat transfer rate q with $\varepsilon_{CO} q_{\max}$. Eq. (12) is taken from Chapter 11 of [23] and Eq. (13) from Chapter 13 of [15].

3.3. Compressor

The compressor model is similar to that of the gas turbine. The equations shown in this Section assume that the inlet and outlet are at states {3} and {4}. It follows that:

$$w_{CP} = h_4 - h_3 = (h_{4s} - h_3) / \eta_{CP} \tag{15}$$

For all the IBC variants that include liquid water drainage, there is no liquid water at the inlet, nor at the outlet because of the increasing temperature. Then Eq. (16) is used to find T_{4s} with the iterative bisection method, where $s^{\circ}_4 - s^{\circ}_3$ is found with Eq. (10), and $h_{4s} - h_3$ is calculated with Eq. (8).

$$R \ln \left(P_4 / P_3 \right) = s^{\circ}_4 - s^{\circ}_3 \tag{16}$$

Regarding the basic IBC, liquid water may be present in the compressor. The entropy of formation of water must then be used in the developed form of Eq. (16):

$$\begin{aligned} R\ln\left(P_4/P_3\right) = & \sum_{i=CO_2,N_2} mf_i \Delta s_i\left(T_{4s},T_3\right) + mf_{Ar}c_{p,Ar}\ln(T_{4s}/T_3) \\ & + mf_{out,vap}\left(s^{\circ}_{f,vap} + \Delta s_{vap}(T_{4s},T_{ref})\right) \\ & - mf_{in,vap}\left(s^{\circ}_{f,vap} + \Delta s_{vap}(T_3,T_{ref})\right) \\ & + mf_{out,liq}\left(s^{\circ}_{f,liq} + s(T_{4s},P_{atm}) - s(T_{ref},P_{atm})\right) \\ & - mf_{in,liq}\left(s^{\circ}_{f,liq} + s(T_3,P_2) - s(T_{ref},P_{atm})\right) \end{aligned} \tag{17}$$

where T_{4s} is the only unknown. Similarly, $h_{4s} - h_3$ is computed using the enthalpy of formation of water. Eqs. (15) and (16) are taken from Chapters 9 and 12 of [15].

3.4. Steam turbine

The steam turbine is the main equipment of the open Rankine cycle in the IBC/D/S and IBC/D/S/R. A representation of the water evolution in the steam turbine between states {9} and {10} is provided in Fig. 6. Differential thermodynamic evolution (see Ref. [26] for more details) is used to model the evolution. Each turbine stage deals with a small part of the total pressure drop, allowing the calculation of the vapor quality at each stage to determine the appropriate efficiency expression to use. When the water is superheated (open squares in Fig. 6), the enthalpy h_j at the outlet of the turbine stage j can be expressed as:

$$h_j = h_{j-1} - \eta_{dry}(h_{j-1} - h_{j,s}) \tag{18}$$

where η_{dry} is the dry efficiency [24]. When the water is a saturated mixture (black squares in Fig. 6), the enthalpy h_j at the outlet of stage j uses the Baumann expression [24] [25]:

$$\begin{aligned} h_j &= \frac{h_{j-1} - A\left(x_j - h_{j,f}\Big/\left(h_{j,g} - h_{j,f}\right)\right)}{1 + A\Big/\left(h_{j,g} - h_{j,f}\right)} \\ A &= \frac{\eta_{dry}}{2}\left(h_{j-1} - h_{j,s}\right) \end{aligned} \tag{19}$$

Finally, the steam turbine specific work is expressed by using the enthalpy of the last pressure stage (enthalpy at state {10}):

$$w_{ST} = h_9 - h_{10} \tag{20}$$

3.5. Heat exchangers

Aside from the condenser (CO) that is present in all cycles, there are four other possible heat exchangers: the refrigeration cycle evaporator (EV/R) and condenser (CO/R), and the open Rankine cycle evaporator (EV/S) and condenser (CO/S). They are all counterflow, but temperature calculations for these pieces of equipment are different. Both condensers use the coolant on the cold side, for which the mass flow rate is unknown. Thus, a temperature difference ΔT_{CO} between the hot side outlet (refrigerant or water) and T_A is assumed. However for the CO/S, ΔT_{CO} allocates the minimum condensing temperature of the water exiting the steam turbine, the minimum vapor quality ultimately deciding the outlet temperature (see constraints in Eqs. (26) and (30)). Furthermore, the EV/S is divided in three parts for calculation purposes (economizer, evaporator and superheater), see Ref. [27]. The economizer and evaporator are constrained by a maximum effectiveness $\varepsilon_{\max}$, while the water state at the outlet of the superheater (SH) is determined using $\varepsilon_{\max}$. The limiting side being always the water, the enthalpy at the steam turbine inlet (state {9}) may be calculated as follow (Chap. 11 of [23]):

$$\begin{aligned} q_{SH} &= h_9 - h_{g@P_9} = \varepsilon_{\max} q_{\max} \\ q_{\max} &= h_{9'} - h_{g@P_9} \\ h_9 &= h_{g@P_9} + \varepsilon_{\max}\left(h_{9'} - h_{g@P_9}\right) \end{aligned} \tag{21}$$

where $h_{g@P_9}$ is the enthalpy of the saturated vapor at pressure P_9 and $h_{9'}$ is the superheated vapor enthalpy if it could reach T_2, (equivalent to an effectiveness of 100%, see Fig. 7a). As an additional verification, the pinch point temperature difference (ΔT_{pp}) located at the economizer output must be higher than a tolerance value ΔT_{tol}. Finally, the same value ΔT_{tol} (see Fig. 7b) is imposed in the EV/R between the refrigerant input and exhaust gases output.

3.6 Fixed parameters

Fixed parameters are listed in Table 1. Turbomachinery efficiencies have been selected based on typical values used in literature. For example, a gas turbine efficiency of 0.795 has been reported in Ref. [2] and compressor efficiency of 0.78 in Ref. [28] in a Brayton cycle. Bianchi and De Pascale [12] used turbomachinery efficiency of 0.8 for the IBC. Steam turbine and pump isentropic efficiencies of 0.75 and 0.85 were chosen in Ref. [3] for a Rankine steam bottom cycle. Vaja et al. [29] state that turbines in ORC have efficiency ranging between 0.8 and 0.88, and use a pump efficiency of 0.8.

Table 1. Values of the fixed parameters in this study.

Parameter	Values
Exhaust gases inlet pressure P_1	101.325 kPa
Gas turbine efficiency η_{GT}	0.8
Compressors efficiency η_{CP}	0.75
Pumps efficiency η_{PP}	0.75
Steam turbine dry efficiency η_{ST}	0.75
Minimum tolerated vapor quality x_{tol}	0.9
Condenser (CO) effectiveness ε_{CO}	0.85
Maximum heat exchanger effectiveness $\varepsilon_{\max}$	0.85
Minimum temperature difference ΔT_{tol}	5 K
Temperature difference CO/S and CO/R ΔT_{CO}	10 K
Range of exhaust gases temperature T_1	600 – 1200 K
Range of coolant temperature T_A	280 – 340 K

4. Optimization

To properly compare the performance of the different thermodynamic cycles, their operation parameters must be optimized. The objective function used in the present study is the specific work output w, which represents the amount of energy (kJ) produced for each kg of exhaust gases. Other

commonly used objective functions include the net power generated, thermal efficiency, exergy destruction and second-law efficiency. Using the specific work as an objective function provides a convenient "reusability" of the results for different exhaust gases mass flow rate. Objective function evaluation, design variables and constraints definition for the five cycles are provided below. Three optimization algorithms have been tested: the function *fmincon.m* with the "interior-point" algorithm, the genetic algorithm function *ga.m*, both from the Optimization Toolbox™ of MATLAB, and an in-house Particle Swarm Optimization (PSO) function. The first algorithm (*fmincon.m*) needed starting points very close to the optimum in order to converge towards it, making the optimization problematic. The second one (*ga.m*) provided better results, but often gave local maxima. PSO was the best to find near-optimum, thus it was selected for this work. Originally developed by Kennedy [30], the PSO algorithm has been implemented in MATLAB based on [31] for the basic principles and [32] to consider constraints. The PSO parameters are: (i) stop criterion: relative error of 10^{-5} between iterations j and $j-2$; (ii) maximum number of iterations: 30; (iii) swarm size: $35 \cdot n_{dv}$, where n_{dv} is the number of design variables; (iv) inertia coefficient: 1; (v) damping coefficient: 0.7; (vi) personal acceleration coefficient: 1; (vii) social acceleration coefficient 1.25. Three optimization runs were done systematically for each set of T_1 and T_A, and in the end, the run with the highest maximized specific work was retained.

The optimization problems described below are relatively "heavy". For optimizing the most complex cycle, ~45 minutes of computational time is required for a single value of T_A and T_1. Since the optimization was repeated for a large number of combinations of T_A and T_1 (1891 scenarios for each cycle, i.e. 31 T_A values × 61 T_1 values), the computational time required was over 175 days for optimizing all the cycles. The complexity comes from to the iterative processes in the calculation of the objective function and the presence of many local maxima.

4.1. IBC and IBC/D optimization

The design variable involved in the optimization of the IBC or the IBC/D is the gas turbine outlet pressure P_2 (see Fig. 1). However, the evaluation of the objective function is different for both:

IBC: $$w = w_{GT} - w_{CP} \tag{22}$$

IBC/D: $$w = w_{GT} - (1 - mf_{H_2O,liq}) w_{CP} - mf_{H_2O,liq} w_{PP} \tag{23}$$

The optimization statement of both cycles can be summarized as:

$$\begin{matrix}\text{IBC} \\ \textit{and} \\ \text{IBC/D}\end{matrix} \begin{cases} \text{maximize}\left(w\right) \\ \text{optimizing}\left(P_2\right) \\ \text{respecting}\left(T_3 - T_A \geq \Delta T_{tol}\right) \\ \text{fixed values: see Table 1} \end{cases} \tag{24}$$

There is only one constraint: the temperature difference in the condenser (CO) between the gas stream outlet and the coolant inlet must be greater than a minimum value ($\Delta T_{tol} = 5$ K).

4.2. IBC/D/S optimization

The IBC/D/S has two design variables: the gas turbine outlet pressure P_2 and the steam turbine inlet pressure P_9 (see Fig. 3). Its specific work output is expressed by

$$w = w_{GT} - (1 - mf_{H_2O,liq}) w_{CP} + mf_{H_2O,liq} (w_{ST} - w_{PP1} - w_{PP2}) \tag{25}$$

while the optimization problem is formulated by

$$\text{IBC/D/S} \begin{cases} \text{maximize}\left(w\right) \\ \text{optimizing}\left(P_2, P_9\right) \\ \text{respecting} \begin{cases} T_4 - T_A \geq \Delta T_{tol}, & x_{\min} \geq x_{tol} \\ \Delta T_{pp} \geq \Delta T_{tol}, & \varepsilon_{EC} \leq \varepsilon_{\max} \\ h_9 \geq h_{g@P_9}, & \varepsilon_{EV} \leq \varepsilon_{\max} \end{cases} \\ \text{fixed values: see Table 1} \end{cases} \tag{26}$$

Six constraints limit the optimization. The first is as in Section 4.1. The five other constraints concern the open Rankine cycle. First, the pinch point temperature difference ΔT_{pp} must be greater than ΔT_{tol}, and the water at state {9} has to be superheated ($h_9 \geq h_{g@P_9}$). Next, each stage of the steam turbine (see in Section 3.4) must have a vapor quality greater than $x_{tol} = 0.9$ to avoid excess

blade wear [15]. Finally, since the efficiencies of the economizer and evaporator are not fixed, they must not exceed a maximum value ($\varepsilon_{\max} = 0.85$).

4.3. IBC/D/R optimization

The IBC/D/R has two design variables: the gas turbine outlet pressure P_2 and the refrigeration utilization rate U_R. The latter is such that when T_4 (see Fig. 4) is equal to T_3, then $U_R = 0$, and when T_4 is equal to 273.2 K, then $U_R = 1$. The objective function is

$$w = w_{GT} - (1 - mf_{H_2O,liq}) w_{CP} - mf_{H_2O,liq} (w_{PP}) - w_{CP/R} \tag{27}$$

and the optimization problem is

$$\text{IBC/D/R} \begin{cases} \text{maximize}\left(w\right) \\ \text{optimizing}\left(P_2, U_R\right) \\ \text{respecting} \begin{cases} T_3 - T_A \geq \Delta T_{tol} \\ P_a \leq P_b \end{cases} \\ \text{fixed values: see Table 1} \end{cases} \tag{28}$$

The first constraint is as in Section 4.1. The second constraint ensures that the compressor (CP/R) inlet pressure P_a is lower than its outlet pressure P_b. The limit is $P_a = P_b$ (no refrigeration).

4.4. IBC/D/S/R optimization

The IBC/D/S/R optimization involves three design variables: the gas turbine outlet pressure P_2, the steam turbine inlet pressure P_9 (see Fig. 5) and the refrigeration utilization rate U_R. The specific work output of the IBC/D/R/S is calculated with

$$w = w_{GT} - (1 - mf_{H_2O,liq}) w_{CP} + mf_{H_2O,liq} (w_{ST} - w_{PP1} - w_{PP2}) - w_{CP/R} \tag{29}$$

and the optimization problem is

$$\text{IBC/D/S/R}\begin{cases}\text{maximize}\left(w\right)\\ \text{optimizing}\left(P_2, P_9, U_R\right)\\ \text{respecting}\begin{cases}T_4 - T_A \geq \Delta T_{tol}, & \varepsilon_{EC} \leq \varepsilon_{\max}\\ \Delta T_{pp} \geq \Delta T_{tol}, & \varepsilon_{EV} \leq \varepsilon_{\max}\\ h_9 \geq h_{g@P_9}, & P_a \leq P_b\\ x_{\min} \geq x_{tol}, & \end{cases}\\ \text{fixed values: see Table 1}\end{cases} \tag{30}$$

Constraints limiting the optimal design combine the ones for the IBC/D/S and for the IBC/D/R.

Table 2. Bounds of the different design variables.

Design variable	Inferior limit	Superior limit
Gas turbine outlet pressure P_2	10 kPa	101.325 kPa
Steam turbine inlet pressure P_9	50 kPa	22 000 kPa
Refrigeration utilization rate U_R	0	1

5. Results

5.1. Parametric analysis of the IBC and IBC/D

In order to illustrate the optimization opportunity of IBC, Fig. 8 presents a parametric analysis of the specific work w with respect to the design variable P_2 for the IBC and IBC/D systems at a given operating condition (i.e., $T_1 = 800$ K and $T_A = 290$ K). The dotted lines in the curves between 16 and 20 kPa indicate the non-respect of the sole condition constraining both cycles (see Eq. (24)) for the pressure P_2. For lower pressures, there is no condensed water, so the specific work output w does not vary between cycles. First, Fig. 8 shows that an optimum exists for both cycles. It can be noted that $w_{\max}$ of IBC/D is located at a higher value of P_2 than $w_{\max}$ of IBC (36.5 vs. 28.0 kPa) for this case. This is due to the amount of condensed water increasing with P_2, thus increasing the drainage before the compressor. However, w starts decreasing after $P_{2,\text{opt}}$ because the reduced flow rate in the compressor does not make up for the decreased power produced in the gas turbine.

Finally, the negative specific work arising from pressure lower than 16 kPa is justified by the equipment being non-isentropic, i.e., less power is produced by the gas turbine while more power is required by the compressor, resulting in the possibility of a negative net specific work.

5.2. Complete optimization results

The optimization methodology described in Section 4 was used to generate the charts presented in Figs. 9 and 10. More specifically, the maximized specific work output $w_{\max}$ for each cycle is shown in Fig. 9 and the corresponding optimized design variables are displayed in Fig. 10. Hence, a total of 1891 optimization runs were performed for each cycle, and each datapoint in the charts is the output of an individual optimization for a couple of T_1 (y-axis) and T_A (x-axis) values.

Figure 9 shows several behaviors of the cycles depending on both temperatures. First, the dotted line in the graphs of the (a) IBC, (b) IBC/D, and (c) IBC/D/S divides the area where there is liquid water drainage (below) and where there is none (above). Indeed, the lower T_1 and T_A, the more condensate there is. Notice that there is a section right below the dotted line where $w_{\max}$ of IBC and IBC/D is comparable. The liquid water drainage is particularly small there, making no noticeable difference between both cycle performances. However, the combined effect of the removed condensate and the supplementary power produced in the steam turbine can be observed in Fig. 9c. The contour lines are more 'horizontal' than in the other cycles which means that $w_{\max}$ is more strongly dependant on T_A (which determines the condensate mass) than on T_1.

Furthermore, it should be observed that the value of $w_{\max}$ for the IBC/D is not always higher than that of the IBC when there is possible condensate drainage. For example, $w_{\max} = 159.6$ kJ/kg for IBC and $w_{\max} = 155.6$ kJ/kg for IBC/D at $T_1 = 1200$ K and $T_A = 280$ K. As a rule of thumb, for value of T_1 above 970 K, keeping liquid water in the compressor leads to a better performance. These results are in line with recent literature [33] [34] indicating that the use of water sprays in the compressor proves to decrease its power consumption for certain cases.

Next, it can be observed in Fig. 9 that the addition of the refrigeration cycle is beneficial for all operating temperatures. The IBC/D/R (Fig. 9d) does not make a significant difference

compared to the IBC/D below the dotted line, but it allows doubling the specific work above the dotted line, where there was originally no condensation. Regarding the IBC/D/S/R, Fig. 9e shows that the combination of an open Rankine cycle with a refrigeration cycle makes it the most performant cycle of the five presented here, for the whole range of operating temperatures.

Finally, Fig. 9f shows the specific energy content of the exhaust in kJ per kg of exhaust as a function of T_A and T_1. This figure is presented in order to convert the specific work output into thermal efficiency, which is another metrics often used to assess the performance of cycles such as IBC. To determine the thermal efficiency of a cycle, its specific work output should be divided by the specific energy content of the exhaust from Fig. 9f. For example, it is found that the thermal efficiency of the IBC/D/S/R varies from 1% (for low hot source temperature and high cold source temperature) to 25% (for high hot source temperature and low cold source temperature).

5.3. Comparison with Rankine cycle and Organic Rankine Cycle

In Section 5.2, the IBC/D/S/R was identified as the best performing cycle of the five presented in this work for the operating conditions investigated. In order to compare its potential to other more 'classical' cycles, the subcritical Rankine cycle (with water) and the subcritical ORC with isobutane ($T_1 < 540$ K) and benzene ($T_1 > 540$ K) have also been simulated and optimized.

The Rankine cycle is the basic steam cycle for power generation, often used as a bottoming cycle for the Brayton Cycle. The ORC is a Rankine cycle using an organic fluid instead of water as working fluid, usually more suitable for heat sources with lower temperatures. Their most simple version consists of a steam turbine to produce work, a condenser to return the fluid to saturated liquid, a pump to reach the evaporating pressure, and a heater (heat exchanger in the context of a WHR system) to obtain the desired thermodynamic state at the turbine inlet. This work employs the same calculation methods found in Section 3.5 for all heat exchangers (economizer, evaporator, superheater and condenser) and in Section 3.4 for the steam turbine.

Results of the present model have been compared with those of two other studies for specific operation points to validate the Rankine cycles model. In the first study, Larsen et al. [35]

compared optimized design performance for Rankine cycle and ORC with R245ca. The selected conditions are ambient air temperature of 298 K and exhaust gases temperature of 507 K, where the engine loaded at 85% leads to an exhaust mass flow of 46.2 kg/s. Although benzene is the working fluid used in Fig. 11b for an exhaust temperature of 507 K, maximized specific work with R245ca has been calculated for comparison purposes. R245ca was not considered here due to its maximum temperature of applicability of 450 K. Table 3 shows that results are fairly similar. Sources of discrepancy include, inter alia, higher component efficiency and higher minimum approaches used in Larsen et al. In the second comparison, an ORC performance using isobutane is taken from Bianchi and De Pascale [12]. Since their specific work is based on the working fluid flow rate, the efficiency based on the available exhaust heat is used instead (Fig. 12). With exhaust temperature of 423 K and ambient air temperature of 288 K, one finds an efficiency of 0.62. Comparing to the results of the present model, which calculated 0.65, the relative difference is found to be 4.8%. Based on these comparisons, the present Rankine cycle models were thus found to be adequate.

Table 3. Specific work comparison with Larsen et al. (2014) for Rankine cycles

Working fluid	Water	R245ca
Net power (Larsen) [kW]	863	1160
Specific work (Larsen) [kJ/kg]	18.68	25.11
Specific work, present model [kJ/kg]	17.45	26.82
Relative difference [%]	6.6	6.8

The operating conditions investigated in this section are an exhaust temperature T_1 from 400 to 1000 K for the Rankine cycle, from 400 to 700 K for the ORC, and a coolant temperature range T_A from 280 to 340 K. The different range for T_1 (400 to 1000 K) has been selected in order to focus on conditions for which the IBC/D/S/R is better than the ORC or the Rankine cycle. Figure 11 shows the ratio between $w_{\max}$ for the IBC/D/S/R and that for (a) ORC $w_{\max}$, and (b) Rankine cycle $w_{\max}$.

In Fig. 11a, it can be observed that the IBC/D/S/R offers a better performance than the ORC with benzene in the specific area, i.e., for T_1 values between 550 and 700 K, and T_A values between 280 and 310 K. Moreover, there are two other identified areas where the IBC/D/S/R is better (for lower T_1 values). In Fig. 11b, the area where the IBC/D/S/R is better than the Rankine cycle is also revealed, i.e., for T_1 values between 400 and 800 K, and T_A values between 280 and 330 K.

5.4. Sensitivity analysis with respect to efficiency of turbomachinery

In the precedent sections, the efficiency of turbomachinery components were fixed to the values in Table 1. However, the overall cycle performance can be affected by these values [36], and therefore a sensitivity analysis is proposed in this Section. One specific test case was chosen for this purpose. The cycles were optimized as previously described, but with different values of efficiencies. Figure 12 shows the maximized specific work output as a function of the efficiency of (a) compressor(s), (b) gas turbine, and (c) steam turbine when applicable for $T_1 = 800$ K and $T_A = 310$ K. For each graph, the efficiency of the piece of equipment is varied between 0.5 and 0.9 while all other parameters remain fixed.

Figures 12a and 12b show that IBC/D/S is the least affected when the compressor and gas turbine efficiency decreases, since it can rely more and more on the steam turbine to produce work with an increased gas turbine outlet pressure P_2. IBC and IBC/D are affected similarly by a change of compressor and/or gas turbine efficiency. Also, as these efficiency values are decreased, the performance of IBC/D/R eventually becomes equivalent to that of IBC and IBC/D up to a point where not work can be produced when the compressor or the gas turbine efficiency value reaches ~0.5. IBC/D/S/R is also affected by the efficiency values, but continues to yield a significant work output even at low efficiency values.

The relatively low impact of the steam turbine efficiency in Fig. 12c may be explained by the optimized pressures and the different path taken by the steam. With a low efficiency, the preferred design is a slightly higher P_2 to obtain hotter steam and a much higher steam turbine inlet pressure P_8. Referring to the water T-s diagram, the steam entropy increases more at each turbine

stage, traveling further to the right and stays superheated at a lower pressure. The vapor quality constraint ($x_{\min} \geq 0.9$) is then respected everywhere in the turbine and the steam exits at the pressure imposed by the condenser, the greater pressure drop compensating for the poor efficiency.

5.5. Parametric analysis of liquid water addition in the IBC/D/S/R

The separated liquid water mass is a limiting factor for the work generation in the IBCs with a steam turbine. If there is additional water available in certain applications, for example an engine in a boat, it would then be possible to mix this supplied water with the one that has been separated from the exhaust stream. Then, in this Section, the supplied water mass per kg of exhaust gases becomes a new design variable, noted as m_{sw}. Figure 13a presents the IBC/D/S/R+ system, the symbol + meaning that supplied water is present.

For each value of m_{sw}, this IBC/D/S/R+ system was optimized with respect to the remaining design variables (P_2, P_9, U_R). The result for each m_{sw} value are presented in Fig. 13b, for two distinct cases (i.e., Case #1: $T_1 = 800$ K, $T_A = 290$ K, and Case #2: $T_1 = 1100$ K, $T_A = 320$ K).

Regarding case #1, it is possible to increase the specific work by a maximum of 23.8% compared to the case without supplied water (i.e., IBC/D/S/R). The maximum is reached at $m_{sw(\text{opt})} = 0.068$, and above this value, $w_{\max}$ decreases and becomes even lower than the IBC/D/S/R work. Regarding case #2, it is possible to increase the specific work by a maximum of 132% compared to the IBC/D/S/R. The maximum is reached at $m_{sw(\text{opt})} = 0.207$. For both cases, it was observed that the optimal value of P_2 is almost equal to P_1, which means that there is almost no work performed by the gas thermodynamic cycle. In other words, the system becomes the equivalent of a Rankine cycle only.

6. Example of applications

Two concrete scenarios are presented to show how to use the results of this paper. In the first scenario, a diesel engine in a truck rejects exhaust gases with a mean temperature of 800 K and the coolant is the ambient air at 300 K. The basic IBC would supply a maximum specific work of 30 kJ/kg (see Fig. 9a); the IBC/D, 31 kJ/kg (Fig. 9b); the IBC/D/S, 53 kJ/kg (Fig. 9c); the IBC/D/R,

38 kJ/kg (Fig. 9d); and the IBC/D/S/R, 100 kJ/kg (Fig. 9e). The best cycle to select would then depend on an economic trade-off between the cost to the different pieces of equipment and the value of the additional work produced by the selected waste heat recovery cycle. The associated operating parameters of the best cycle (IBC/D/S/R) are $P_{2(\text{opt})} = 45$ kPa (see Fig. 10g), $P_{9(\text{opt})} = 3.6$ MPa (Fig. 10h), and $U_{R(\text{opt})} = 0.84$ (Fig. 10i). However, Fig. 11b shows that the Rankine cycle is a better choice for that scenario, where the optimal IBC/D/S/R yields to less than 70% of the optimal Rankine cycle performance.

In the second scenario, a reciprocating diesel engine in a container carrier rejects exhaust gases with a mean temperature of 600 K and the coolant is the sea water at its surface mean temperature, 290 K [37]. The basic IBC would supply a maximum specific work of less than 1 kJ/kg (see Fig. 9a); the IBC/D, 8 kJ/kg (Fig. 9b); the IBC/D/S, 49 kJ/kg (Fig. 9c); the IBC/D/R, 10 kJ/kg (Fig. 9d); and the IBC/D/S/R, 51 kJ/kg (Fig. 9e). The refrigeration cycle having only a weak impact on the performance for this scenario, the IBC/D/S could be a better choice than the IBC/D/S/R. However, this 4% improvement might be enough to justify the supplementary equipment, especially in a container carrier where the weight is less of a constraint than on land. The associated operating parameters of the IBC/D/S are $P_{2(\text{opt})} = 90$ kPa (see Fig. 10b) and $P_{9(\text{opt})} \approx 1$ MPa (Fig. 10c). Both cycles have a better performance than an ORC with benzene: by 15% for the IBC/D/S/R and by 11% for the IBC/D/S (see Fig. 11a).

To get an estimate of what these numbers represent in terms of the nominal engine work, a theoretical diesel cycle is considered. For the truck example, a compression ratio of 18 leads to an engine specific work of 970 kJ/kg. Thus, the IBC/D/S/R would be able to recover heat corresponding to about 10 % of the engine power. For the container carrier example, a compression ratio of 14 leads to an engine specific work of 560 kJ/kg. The IBC/D/S then would provide about 9 % additional power.

While it would be difficult to incorporate in a cost-effective way a system like the IBC/D/S/R in a truck, it could be a more realistic solution in large boats. As stated in Mito et al. [38], reducing maritime transport CO_2 and NO_x emissions calls for less fuel consumed. Large ships

engines usually have exhaust gases colder than in land transportation. Looking at Fig. 9, IBC/D/S and IBC/D/S/R then would make the best use of low exhaust temperature and ocean water temperature as cold sink. In addition to a higher performance in this range of temperatures, an advantage of IBC/D/S over ORC is the absence of an additional working fluid that can be hazardous and environmentally damaging [35]. However, the IBCs are currently designed to exploit only the exhaust waste heat, which can be considered as a drawback when compared to other WHR solutions. Engines have other heat sources like scavenger air and jacket water, which the ORC is capable to recover, see Ref. [39].

7. Conclusion

In this paper, five different Inverted Brayton Cycles are numerically simulated and optimized to various operating conditions (exhaust temperature and coolant temperature). Among these five systems, three are presented for the first time in the literature (i.e., the IBC/D/S, IBC/D/R and IBC/D/S/R). The objective function was the specific work output, and the design variables were the gas turbine outlet pressure (for all cycles), the steam turbine inlet pressure (for IBC/D/S and IBC/D/S/R), and the refrigeration utilization rate (for IBC/D/R and IBC/D/S/R). A PSO script was used to perform the optimization for a range of exhaust temperature from 600 to 1200 K and of coolant temperature from 280 to 340 K.

The optimization results are reported in the form of design charts (Figs. 9 to 11). For instance, the data presented in Figs. 9 and 10 allows to perform the predesign of heat recovery systems using the IBC principle. The addition of a refrigeration cycle to the IBC/D turned out beneficial for all operating conditions, especially for exhaust temperature higher than 700 K Moreover, the data presented in Fig. 11 allows to determine for which operating conditions the IBC/D/S/R may be more efficient than a basic ORC or a Rankine cycle. The sensitivity analysis on turbomachinery efficiencies highlighted the impact they have on overall system performance. Finally, the data presented in Fig. 13 illustrates the effect of adding supplied liquid water after the separation for two specific cases of operating conditions.

The work presented in this paper could be extended in various ways. An economic analysis of the different IBC cycles would be needed to determine to which extent their specific work output justifies their purchase cost in different contexts, compared with other types of cycles. Multi-objective optimization of the IBC cycles including objective functions such as weight, space or cost could help to identify families of optimal solutions best suited for different applications. The models developed for this study could also be improved. For example, the pressure losses and heat losses could be considered, and the transient behavior of the system that results from the variations of hot and cold source temperatures could also be investigated. Such transient behavior would require mathematical expressions of the performance of each piece of equipment in off-design conditions. Moreover, new cycles using water recirculation could be simulated and optimized. For example, water exiting the steam turbine of the IBC/D/S or IBC/D/R/S could be reinjected in the exhaust gases upstream of the gas turbine, which can potentially increase the specific work output of the cycle.

Acknowledgements

The Université Laval authors' work was supported by the Natural Sciences and Engineering Research Council of Canada (NSERC). The first author received the Canadian Queen Elizabeth II Diamond Jubilee Scholarship, which funded her research stay at University of Bath (UK) for one semester during which this work was initiated.

Appendix A

Tables A.1, A.2 and A.3 describe the thermodynamic states in each new cycle proposal for a common case of optimized design at $T_1 = 900$ K and $T_A = 300$ K. The reference state to calculate enthalpy and entropy for the exhaust gases is at $T_{ref} = 298$ K and $P_{ref} = P_{atm}$. Notice that state {4} of IBC/D/S and IBC/D/R, and state {5} of IBC/D/S/R are not included in tables: liquid water and "dry" exhaust gases have each their own state after the separation.

Table A.1. Thermodynamic states of the exhaust gases and separated water in the optimized IBC/D/S system for a specific case.

State	Composition	$\dot{m}/\dot{m}_1$ [%]	T [K]	P [kPa]	h [kJ/kg]	s [kJ/kg·K]
1	Exhaust	100	900.00	101.325	695.515	1.25946
2	Exhaust	100	801.53	54.2602	544.314	1.29776
3	Exhaust	100	754.20	54.2602	517.376	1.22425
5	Exhaust	98.2	310.59	54.2602	13.2834	0.22428
6	Exhaust	98.2	386.07	101.325	93.8581	0.27580
7	Water	1.79	310.59	54.2602	156.881	0.53881
8	Water	1.79	311.47	8184.82	167.797	0.54691
9	Water	1.79	758.46	8184.82	3360.58	6.66594
10	Water	1.79	324.54	13.2313	2382.66	7.40041
11	Water	1.79	324.54	13.2313	215.166	0.72179
12	Water	1.79	324.55	101.325	215.285	0.72188

Table A.2. Thermodynamic states of the exhaust gases, separated water and R134a in the optimized IBC/D/R system for a specific case.

Point	Composition	$\dot{m}/\dot{m}_1$ [%]	T [K]	P [kPa]	h [kJ/kg]	s [kJ/kg·K]
1	Exhaust	100	900.00	101.325	695.515	1.25946
2	Exhaust	100	730.69	32.7641	489.218	1.33222
3	Exhaust	100	319.53	32.7641	23.0570	0.40123
5	Exhaust	94.8	291.79	32.7641	-6.35141	0.30499
6	Exhaust	94.8	429.86	101.325	137.384	0.38130
7	Water	5.24	291.79	32.7641	78.2407	0.27698
8	Water	5.24	291.79	101.325	78.3323	0.27706
a	R134a	56.0	289.79	467.355	409.210	1.73054
b	R134a	56.0	319.74	933.396	428.637	1.74583
c	R134a	56.0	310.00	933.396	251.731	1.17569
d	R134a	56.0	286.79	467.355	251.731	1.18148

Table A.3. Thermodynamic states of the exhaust gases, separated water and R134a in the optimized IBC/D/S/R system for a specific case.

Point	Composition	$\dot{m}/\dot{m}_1$ [%]	T [K]	P [kPa]	h [kJ/kg]	s [kJ/kg·K]
1	Exhaust	100	900.00	101.325	695.515	1.25946
2	Exhaust	100	746.18	36.7553	507.760	1.32409
3	Exhaust	100	525.29	36.7553	250.147	0.91539
4	Exhaust	100	305.00	36.7553	7.41948	0.31789
6	Exhaust	92.1	275.75	36.7553	-23.4923	0.21135
7	Exhaust	92.1	392.65	101.325	95.7856	0.27897
8	Water	7.91	275.75	36.7553	10.9571	0.03979
9	Water	7.91	276.20	5717.26	18.5317	0.04668
10	Water	7.91	710.44	5717.26	3276.11	6.70536
11	Water	7.91	322.95	12.2313	2380.59	7.42694
12	Water	7.91	322.95	12.2313	208.515	0.70125
13	Water	7.91	322.97	101.325	208.652	0.70139
a	R134a	74.6	273.75	268.185	399.850	1.73820
b	R134a	74.6	325.75	933.396	434.990	1.76552
c	R134a	74.6	310.00	933.396	251.731	1.17569
d	R134a	74.6	270.75	268.185	251.731	1.19119

References

[1] Z. Chen, C. Copeland, B. Ceen, S. Jones, and A. A. Goya, "Modeling and Simulation of an Inverted Brayton Cycle as an Exhaust-Gas Heat-Recovery System," *J. Eng. Gas Turbines Power-Trans. Asme*, vol. 139, no. 8, p. 081701, Aug. 2017.

[2] A. Uusitalo, A. Ameli, and T. Turunen-Saaresti, "Thermodynamic and turbomachinery design analysis of supercritical Brayton cycles for exhaust gas heat recovery," *Energy*, vol. 167, pp. 60–79, Jan. 2019.

[3] J. P. Liu, J. Q. Fu, C. Q. Ren, L. J. Wang, Z. X. Xu, and B. L. Deng, "Comparison and analysis of engine exhaust gas energy recovery potential through various bottom cycles," *Appl. Therm. Eng.*, vol. 50, no. 1, pp. 1219–1234, Jan. 2013.

[4] A. T. Hoang, "Waste heat recovery from diesel engines based on Organic Rankine Cycle," *Appl. Energy*, vol. 231, pp. 138–166, Dec. 2018.

[5] D. G. Wilson, "Design of high-efficiency turbomachinery and gas turbines," Jan. 1983.

[6] M. Bianchi, G. N. di Montenegro, A. Peretto, and P. R. Spina, "A feasibility study of inverted brayton cycle for gas turbine repowering," *J. Eng. Gas Turbines Power-Trans. Asme*, vol. 127, no. 3, pp. 599–605, Jul. 2005.

[7] N. Iki, H. Furutani, and S. Takahashi, *Potential of a reheat gas turbine system using inverted Brayton cycle*. New York: Amer Soc Mechanical Engineers, 2005.
[8] M. Bianchi, G. N. di Montenegro, and A. Peretto, "Inverted Brayton cycle employment for low-temperature cogenerative applications," *J. Eng. Gas Turbines Power-Trans. Asme*, vol. 124, no. 3, pp. 561–565, Jul. 2002.
[9] M. Henke, T. Monz, and M. Aigner, "Inverted Brayton Cycle With Exhaust Gas Recirculation-A Numerical Investigation," *J. Eng. Gas Turbines Power-Trans. Asme*, vol. 135, no. 9, p. 091203, Sep. 2013.
[10] M. M. Bailey, "Comparative Evaluation of Three Alternative Power Cycles for Waste Heat Recovery From the Exhaust of Adiabatic Diesel Engines," NASA Lewis Reasearch Center, Cleveland, OH, United States, Technical Report No. NASA-TM-86953, 1985.
[11] S. Fujii, K. Kaneko, K. Otani, and Y. Tsujikawa, "Mirror gas turbines: A newly proposed method of exhaust heat recovery," *J. Eng. Gas Turbines Power-Trans. Asme*, vol. 123, no. 3, pp. 481–486, Jul. 2001.
[12] M. Bianchi and A. De Pascale, "Bottoming cycles for electric energy generation: Parametric investigation of available and innovative solutions for the exploitation of low and medium temperature heat sources," *Appl. Energy*, vol. 88, no. 5, pp. 1500–1509, May 2011.
[13] C. D. Copeland and Z. Chen, "The Benefits of an Inverted Brayton Bottoming Cycle as an Alternative to Turbocompounding," *J. Eng. Gas Turbines Power-Trans. Asme*, vol. 138, no. 7, p. 071701, Jul. 2016.
[14] I. Kennedy, Z. Chen, B. Ceen, S. Jones, and C. D. Copeland, *Inverted Brayton Cycle with Exhaust Gas Condensation*. New York: Amer Soc Mechanical Engineers, 2017.
[15] Y. A. Çengel, M. A. Boles, and M. Lacroix, *Thermodynamique: Une Approche Pragmatique*, Sixth. Montréal: Les Éditions de la Chenelière inc., 2008.
[16] A. Buck, "New Equations for Computing Vapor-Pressure and Enhancement Factor," *J. Appl. Meteorol.*, vol. 20, no. 12, pp. 1527–1532, 1981.
[17] C. Zilio, J. S. Brown, G. Schiochet, and A. Cavallini, "The refrigerant R1234yf in air conditioning systems," *Energy*, vol. 36, no. 10, pp. 6110–6120, Oct. 2011.
[18] MATLAB, "The Mathworks Inc.," 2014.
[19] I. H. Bell, J. Wronski, S. Quoilin, and V. Lemort, "Pure and Pseudo-pure Fluid Thermophysical Property Evaluation and the Open-Source Thermophysical Property Library CoolProp," *Ind. Eng. Chem. Res.*, vol. 53, no. 6, pp. 2498–2508, Feb. 2014.
[20] "Welcome to CoolProp — CoolProp 6.1.0 documentation." [Online]. Available: http://www.coolprop.org/. [Accessed: 08-Oct-2018].
[21] L. J. Gillespie, "The Gibbs-Dalton Law of Partial Pressures," *Phys. Rev.*, vol. 36, no. 1, pp. 121–131, Jul. 1930.
[22] G. B. Arfken, *Mathematical Methods for Physicists*, Third. Orlando: Academic Press, Inc., 1985.
[23] T. L. Bergman, A. S. Lavine, F. P. Incropera, and D. P. Dewitt, *Fundamentals of heat and mass transfer*, Seventh. Hoboken: John Wiley & Sons, Inc., 2011.
[24] R. DiPippo, *Geothermal Power Plants: Principles, Applications, Case Studies and Environmental Impact*, Third. Boston: Butterworth-Heinemann, 2012.
[25] K. Baumann, "Some Recent Developements in Large Steam Turbine Practice," *J. Inst. Electr. Eng.*, vol. 59, pp. 565–623, 1921.
[26] N. Chagnon-Lessard, F. Mathieu-Potvin, and L. Gosselin, "Geothermal power plants with maximized specific power output: Optimal working fluid and operating conditions of subcritical and transcritical Organic Rankine Cycles," *Geothermics*, vol. 64, pp. 111–124, Nov. 2016.
[27] P. K. Nag, *Power Plant Engineering*, Third. New Delhi: Tata McGraw Hill Education Private Limited, 2008.
[28] W. B. Nader, C. Mansour, C. Dumand, and M. Nemer, "Brayton cycles as waste heat recovery systems on series hybrid electric vehicles," *Energy Convers. Manag.*, vol. 168, pp. 200–214, Jul. 2018.

[29] I. Vaja and A. Gambarotta, “Internal Combustion Engine (ICE) bottoming with Organic Rankine Cycles (ORCs),” *Energy*, vol. 35, no. 2, pp. 1084–1093, Feb. 2010.
[30] J. Kennedy and R. Eberhart, “Particle swarm optimization,” in *, IEEE International Conference on Neural Networks, 1995. Proceedings*, 1995, vol. 4, pp. 1942–1948 vol.4.
[31] Yarpiz, “Video Tutorial of PSO implementation in MATLAB,” *Yarpiz*, 23-May-2016. .
[32] J. Clarke, L. McLay, and J. T. McLeskey, “Comparison of genetic algorithm to particle swarm for constrained simulation-based optimization of a geothermal power plant,” *Adv. Eng. Inform.*, vol. 28, no. 1, pp. 81–90, Jan. 2014.
[33] J. GuanWei, C. MaoLin, X. WeiQing, and S. Yan, “Energy conversion characteristics of reciprocating piston quasi-isothermal compression systems using water sprays,” *Sci. China-Technol. Sci.*, vol. 61, no. 2, pp. 285–298, Feb. 2018.
[34] Y. Tian, J. Shen, C. Wang, Z. Xing, and X. Wang, “Modeling and performance study of a water-injected twin-screw water vapor compressor,” *Int. J. Refrig.-Rev. Int. Froid*, vol. 83, pp. 75–87, Nov. 2017.
[35] U. Larsen, O. Sigthorsson, and F. Haglind, “A comparison of advanced heat recovery power cycles in a combined cycle for large ships,” *Energy*, vol. 74, pp. 260–268, Sep. 2014.
[36] B. Deng, Q. Tang, and M. Li, “Study on the steam-assisted Brayton air cycle for exhaust heat recovery of internal combustion engine,” *Appl. Therm. Eng.*, vol. 125, pp. 714–726, Oct. 2017.
[37] “Temperature of Ocean Water - Windows to the Universe.” [Online]. Available: https://www.windows2universe.org/?page=/earth/water/temp.html. [Accessed: 10-Oct-2018].
[38] M. T. Mito, M. A. Teamah, W. M. El-Maghlany, and A. I. Shehata, “Utilizing the scavenge air cooling in improving the performance of marine diesel engine waste heat recovery systems,” *Energy*, vol. 142, pp. 264–276, Jan. 2018.
[39] R. Scaccabarozzi, M. Tavano, C. M. Invernizzi, and E. Martelli, “Comparison of working fluids and cycle optimization for heat recovery ORCs from large internal combustion engines,” *Energy*, vol. 158, pp. 396–416, Sep. 2018.

Figure captions

Figure 1 Inverted Brayton Cycle (IBC). (a) Equipment architecture. (b) Thermodynamic diagram of exhaust gases.

Figure 2 Inverted Brayton Cycle with liquid water drainage (IBC/D). (a) Equipment architecture. (b) Thermodynamic diagram of exhaust gases. (c) Thermodynamic diagram of water.

Figure 3 Inverted Brayton Cycle with liquid water drainage and steam turbine (IBC/D/S). (a) Equipment architecture. (b) Thermodynamic diagram of exhaust gases. (c) Thermodynamic diagram of water.

Figure 4 Inverted Brayton Cycle with liquid water drainage and refrigeration cycle (IBC/D/R). (a) Equipment architecture. (b) Thermodynamic diagram of exhaust gases. (c) Thermodynamic diagram of water. (d) Thermodynamic diagram of refrigerant.

Figure 5 Inverted Brayton Cycle with liquid water drainage, steam turbine and refrigeration cycle (IBC/D/S/R). (a) Equipment architecture. (b) Thermodynamic diagram of exhaust gases. (c) Thermodynamic diagram of water. (d) Thermodynamic diagram of refrigerant.

Figure 6 Calculation principle of steam turbine intermediate stages on thermodynamic diagram.

Figure 7 Temperature evolution in evaporators. (a) EV/S. (b) EV/R.

Figure 8 Parametric analysis of IBC and IBC/D for a specific case.

Figure 9 Maximized specific work output for each cycle. (a) IBC. (b) IBC/D. (c) IBC/D/S. (d) IBC/D/R. (e) IBC/D/S/R.

Figure 10 Optimized design variables for each cycle. (a) IBC $P_{2(\mathrm{opt})}$. (b) IBC/D/S $P_{2(\mathrm{opt})}$. (c) IBC/D/S $P_{9(\mathrm{opt})}$. (d) IBC/D $P_{2(\mathrm{opt})}$. (e) IBC/D/R $P_{2(\mathrm{opt})}$. (f) IBC/D/R $U_{R(\mathrm{opt})}$. (g) IBC/D/S/R $P_{2(\mathrm{opt})}$. (h) IBC/D/S/R $P_{9(\mathrm{opt})}$. (i) IBC/D/S/R $U_{R(\mathrm{opt})}$.

Figure 11 Ratio of the cycles' maximized specific work. (a) Between the IBC/D/S/R and two ORCs. (b) Between IBC/D/S/R and the Rankine cycle.

Figure 12 Maximized specific work output at $T_1 = 800\ \mathrm{K}$ & $T_A = 310\ \mathrm{K}$ with respect to the (a) Compressor(s) efficiency. (b) Gas turbine efficiency. (c) Steam turbine efficiency.

Figure 13 Evolution of the IBC/D/R/S+ $w_{\max}$ with respect to the supplied water mass m_{sw} for case #1 ($T_1 = 800$ K & $T_A = 290$ K) and case #2 ($T_1 = 1100$ K & $T_A = 320$ K).

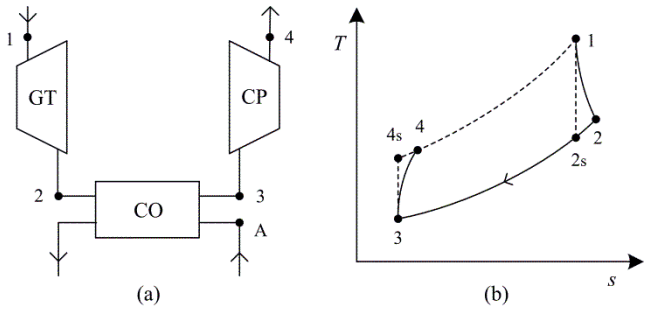

Figure 1

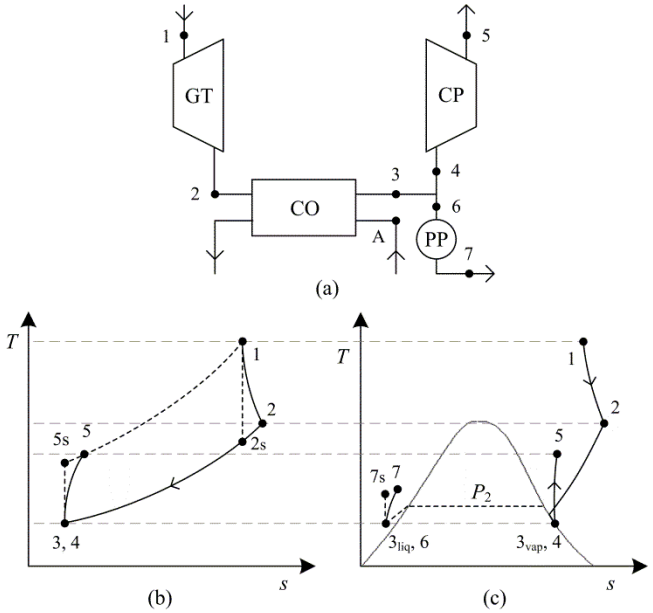
1
GT
5
CP
2
CO
3
4
6
A
PP
7
(a)
T
1
2
5s
5
2s
3, 4
s
(b)
T
1
2
5
7s
7
P_2
3_{liq}, 6
3_{vap}, 4
s
(c)

Figure 2

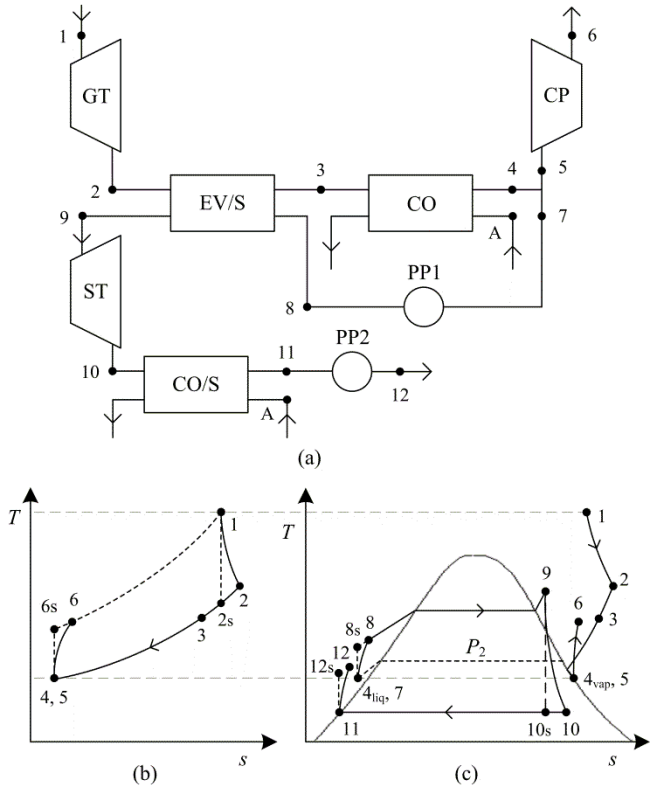
1
GT
6
CP
2
EV/S
3
CO
4
5
9
ST
A
7
PP1
8
PP2
10
CO/S
11
12
A
(a)
T
1
6s
6
2
2s
3
4, 5
s
(b)
T
1
9
2
6
3
8s
8
12
P_2
12s
4_{vap}, 5
4_{liq}, 7
11
10s
10
s
(c)

Figure 3

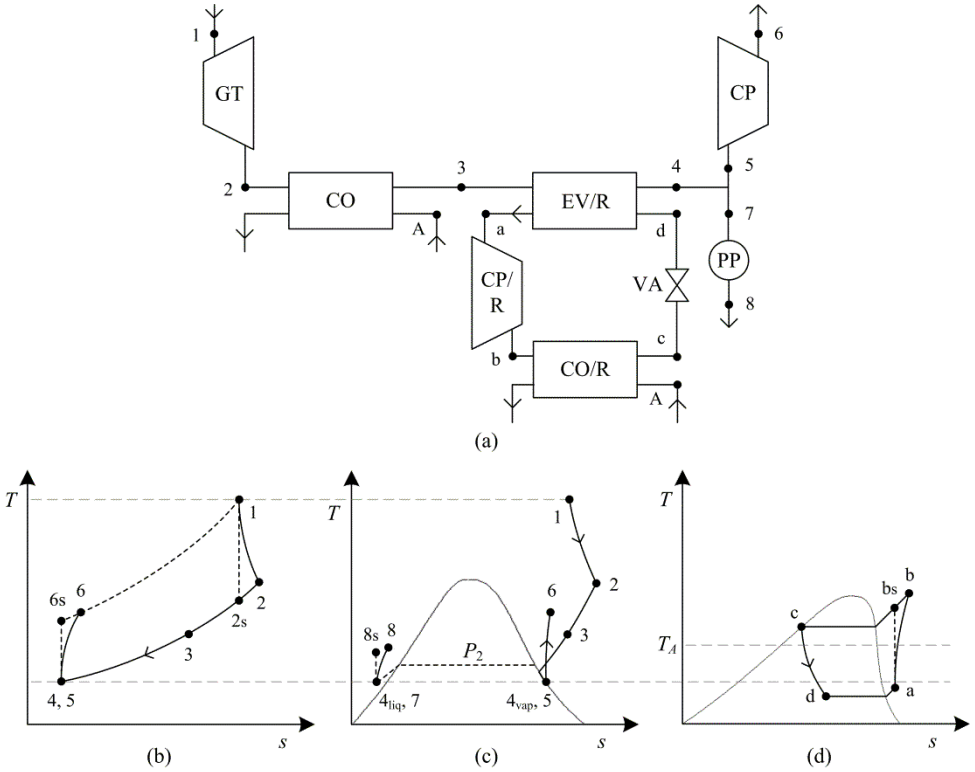
1
GT
2
CO
3
A
EV/R
4
a
d
CP/
R
VA
CP
5
6
7
PP
8
b
c
CO/R
A
(a)
T
1
6s
6
2s
2
3
4, 5
s
(b)
T
1
2
6
3
8s
8
P_2
4_{liq}, 7
4_{vap}, 5
s
(c)
T
b
bs
c
T_A
d
a
s
(d)

Figure 4

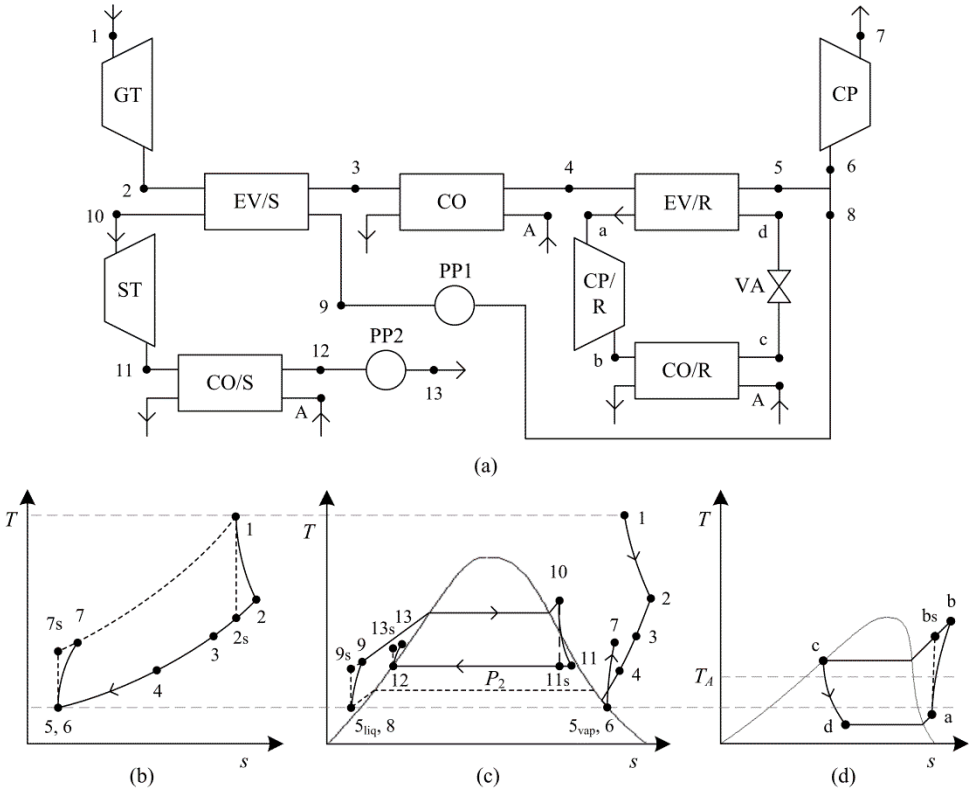
GT
CP
EV/S
CO
EV/R
ST
PP1
CP/
R
VA
PP2
CO/S
CO/R
A
(a)
T
s
5, 6
7s
7
2s
2
3
4
(b)
5liq, 8
5vap, 6
9s
9
13s
13
12
P2
11s
11
10
(c)
TA
bs
b
c
d
a
(d)

Figure 5

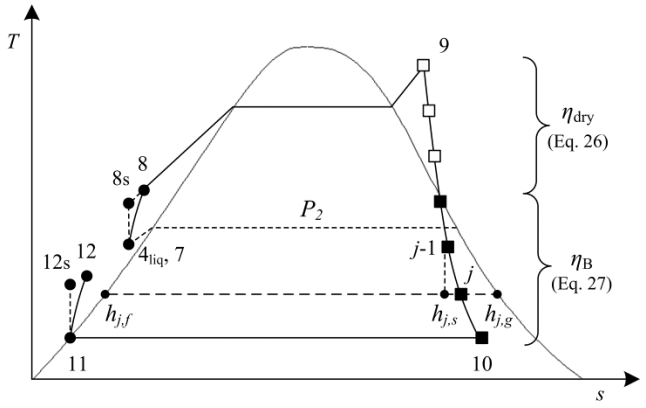
T
9
η_{dry}
(Eq. 26)
8
8s
P_2
12
12s
4_{liq}, 7
j-1
j
η_B
(Eq. 27)
$h_{j,f}$
$h_{j,s}$
$h_{j,g}$
11
10
s

Figure 6

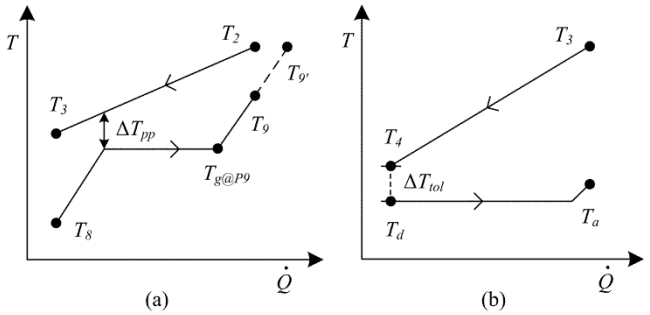
T
T_2
$T_{9'}$
T_3
ΔT_{pp}
T_9
$T_{g@P9}$
T_8
$\dot{Q}$
(a)
T
T_3
T_4
ΔT_{tol}
T_d
T_a
$\dot{Q}$
(b)

Figure 7

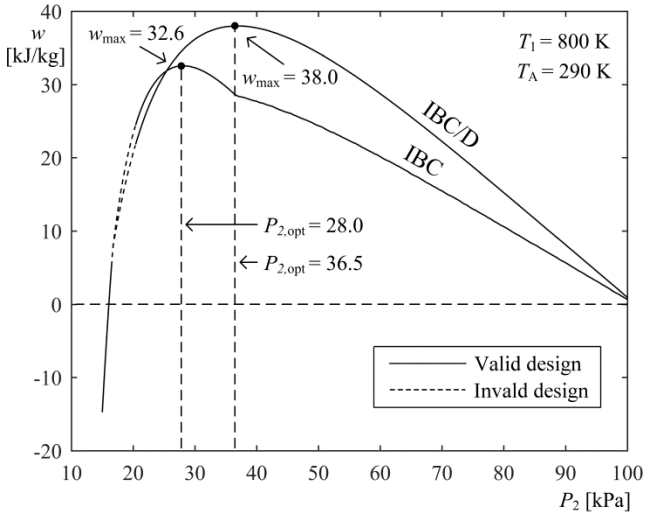
40
w
[kJ/kg]
30
20
10
0
-10
-20
10
20
30
40
50
60
70
80
90
100
P2 [kPa]
wmax = 32.6
wmax = 38.0
T1 = 800 K
TA = 290 K
IBC/D
IBC
P2,opt = 28.0
P2,opt = 36.5
Valid design
Invald design

Figure 8

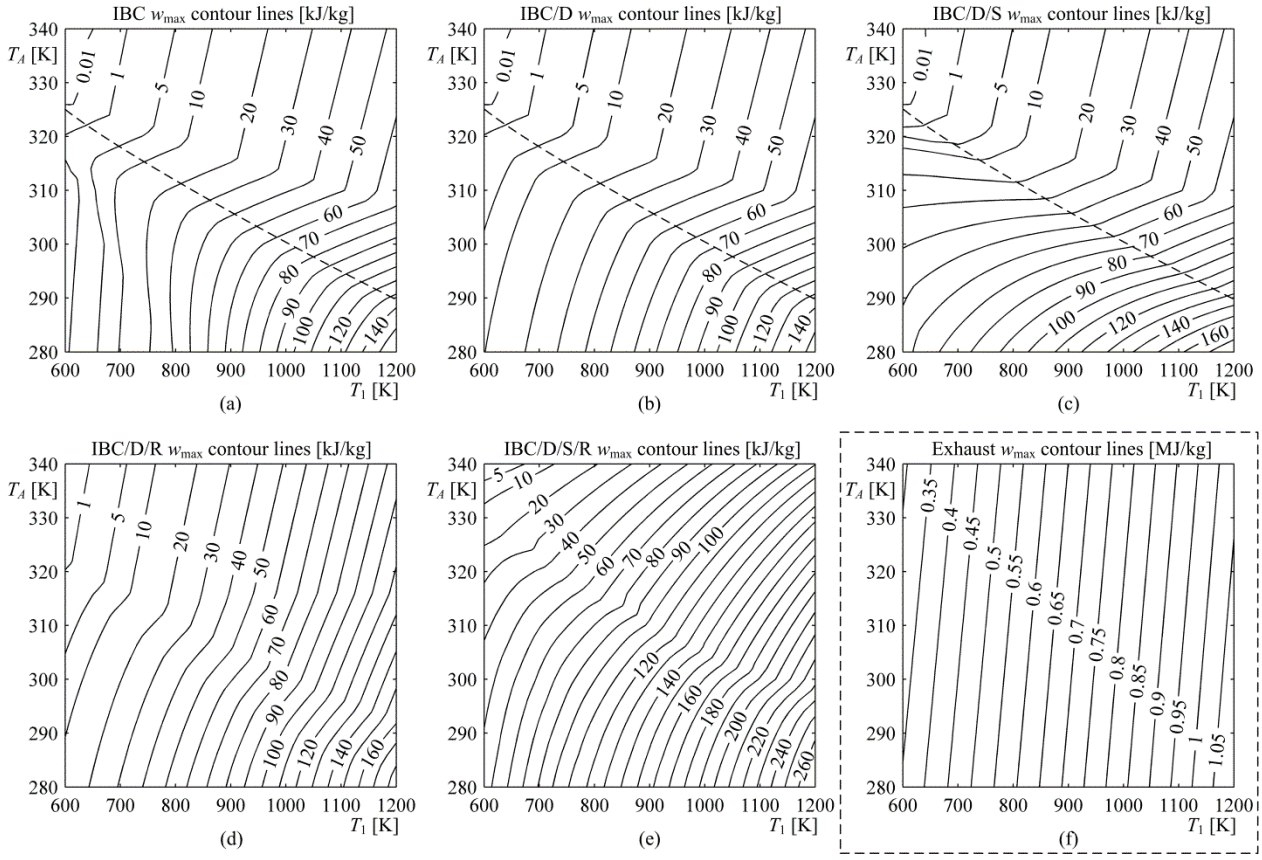
IBC w_{max} contour lines [kJ/kg]
IBC/D w_{max} contour lines [kJ/kg]
IBC/D/S w_{max} contour lines [kJ/kg]
IBC/D/R w_{max} contour lines [kJ/kg]
IBC/D/S/R w_{max} contour lines [kJ/kg]
Exhaust w_{max} contour lines [MJ/kg]
T_A [K]
T_1 [K]
(a)
(b)
(c)
(d)
(e)
(f)

Figure 9

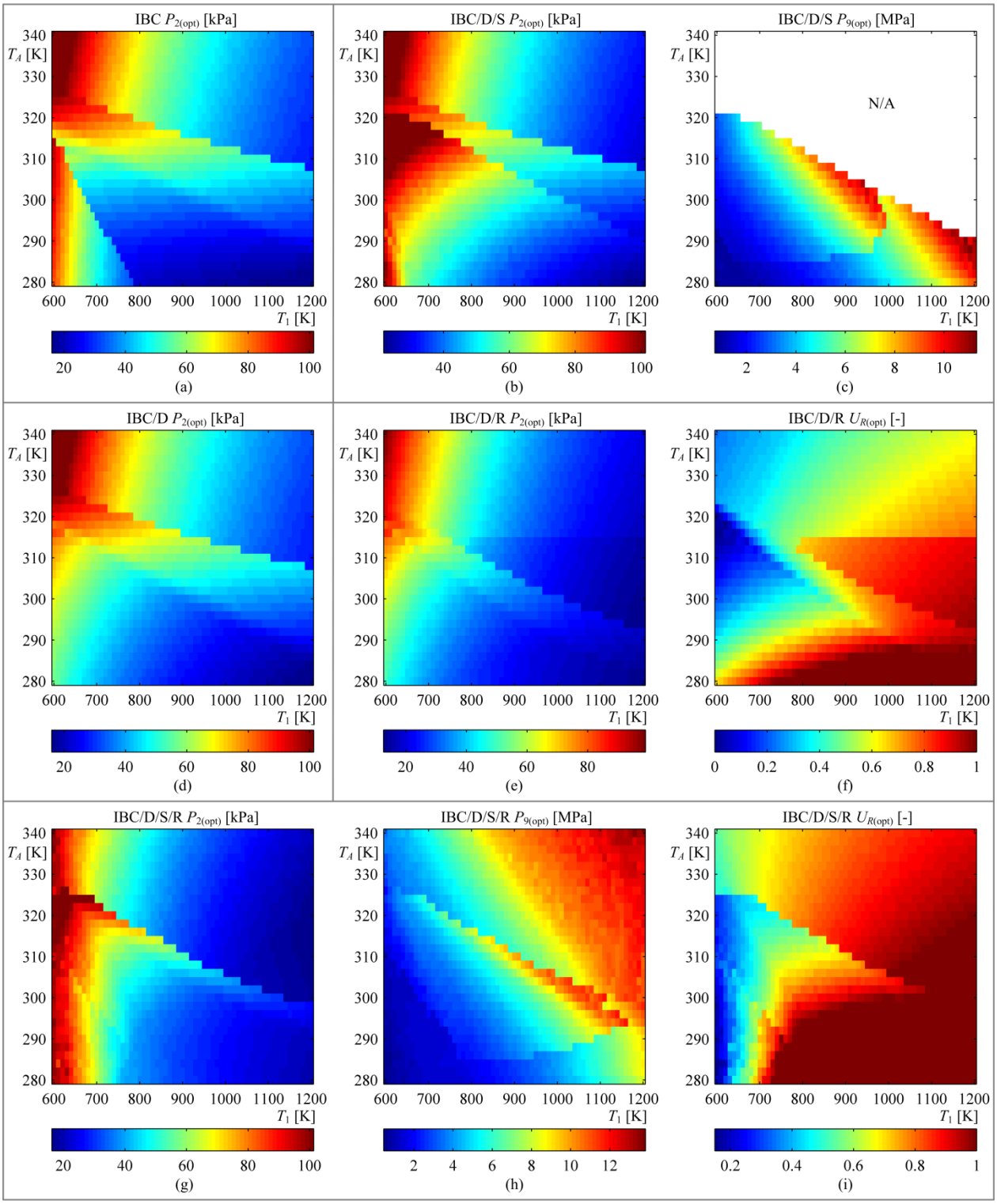
IBC $P_{2(opt)}$ [kPa]
IBC/D/S $P_{2(opt)}$ [kPa]
IBC/D/S $P_{9(opt)}$ [MPa]
N/A
IBC/D $P_{2(opt)}$ [kPa]
IBC/D/R $P_{2(opt)}$ [kPa]
IBC/D/R $U_{R(opt)}$ [-]
IBC/D/S/R $P_{2(opt)}$ [kPa]
IBC/D/S/R $P_{9(opt)}$ [MPa]
IBC/D/S/R $U_{R(opt)}$ [-]
T_A [K]
T_1 [K]
(a)
(b)
(c)
(d)
(e)
(f)
(g)
(h)
(i)

Figure 10

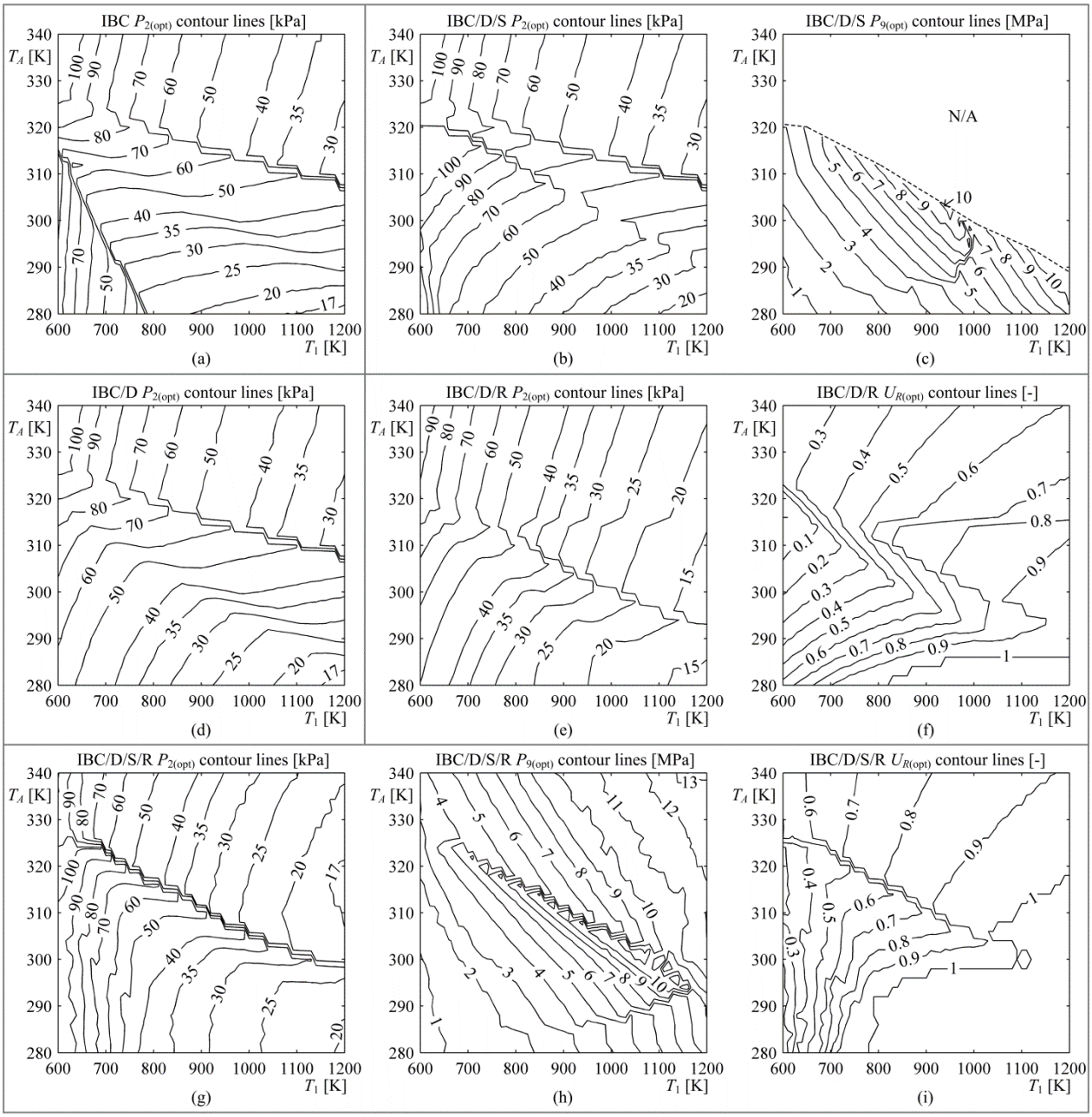

Figure 10 (printable version)

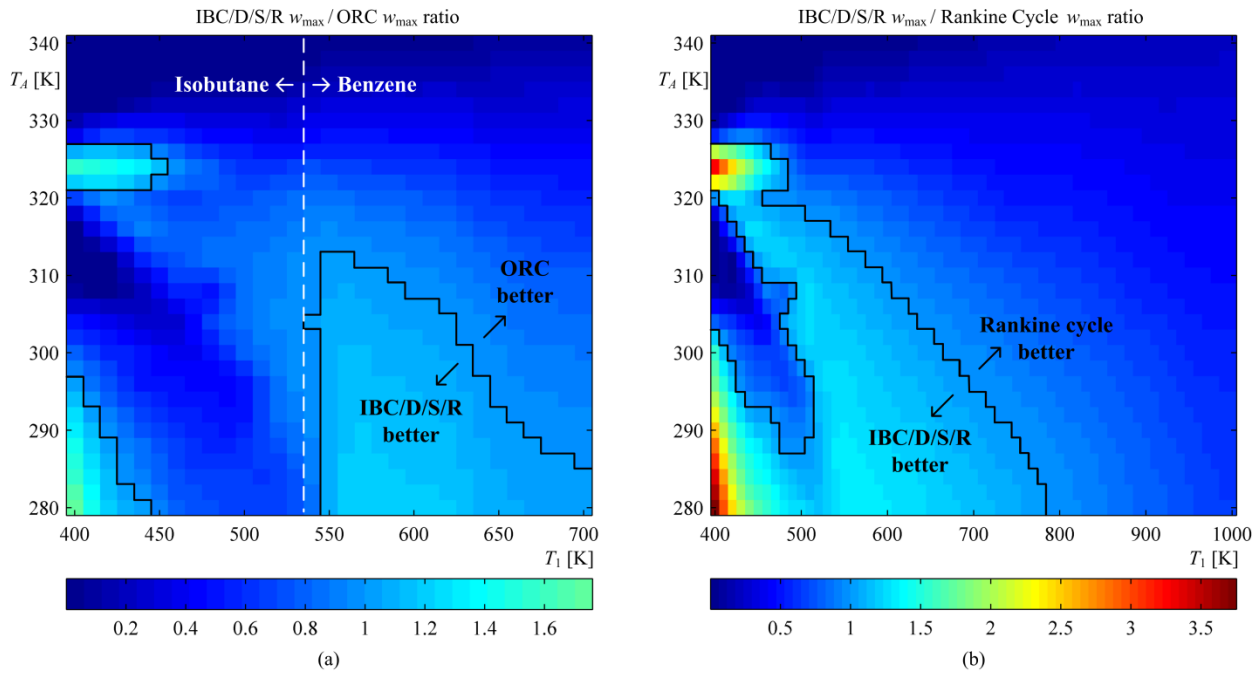

Figure 11

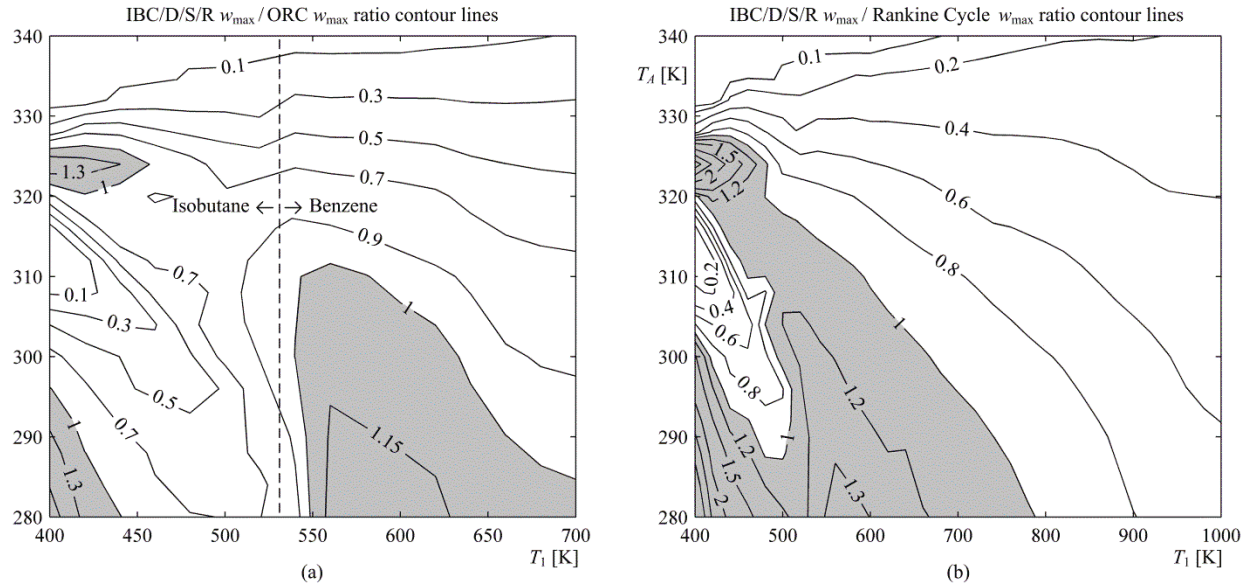

Figure 11 (printable version)

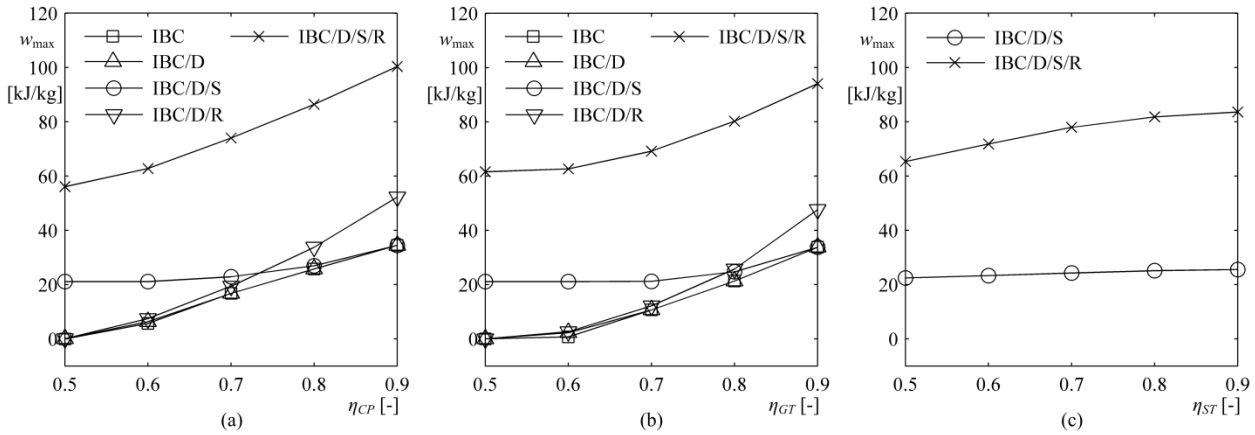
120
w_{max}
[kJ/kg]
100
80
60
40
20
0
IBC
IBC/D
IBC/D/S
IBC/D/R
IBC/D/S/R
0.5
0.6
0.7
0.8
0.9
η_{CP} [-]
(a)
η_{GT} [-]
(b)
IBC/D/S
IBC/D/S/R
η_{ST} [-]
(c)

Figure 12

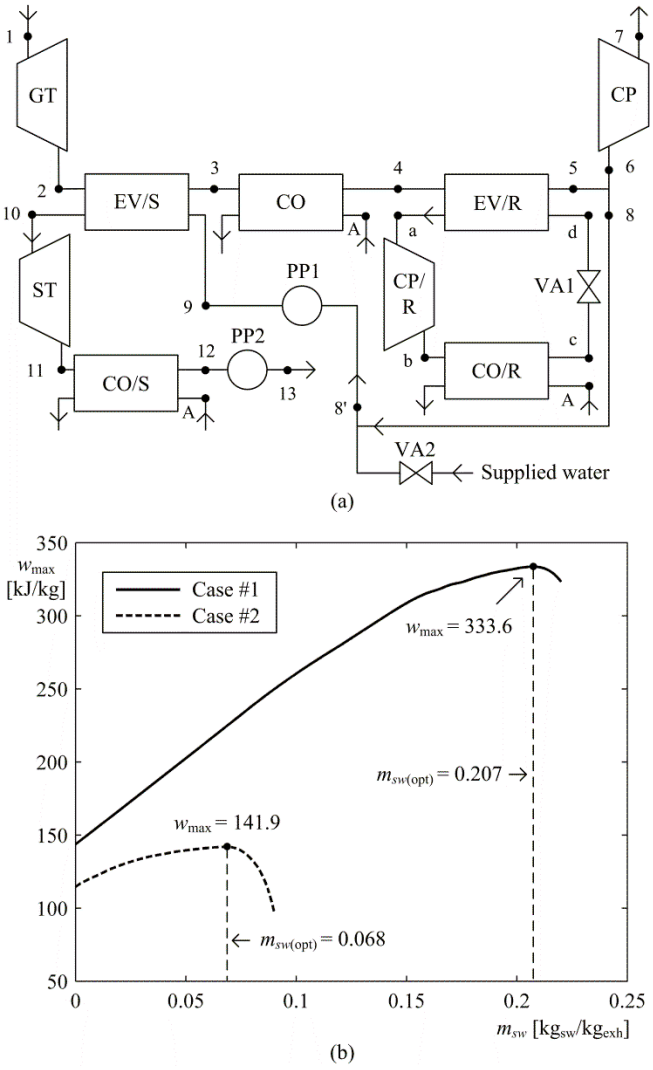
1
GT
7
CP
2
EV/S
3
CO
4
EV/R
5
6
10
A
a
d
8
ST
PP1
CP/
R
VA1
9
PP2
c
12
b
11
CO/S
CO/R
13
8'
A
A
VA2
Supplied water
(a)
350
w_{max}
[kJ/kg]
300
250
200
150
100
50
Case #1
Case #2
w_{max} = 333.6
$m_{sw(opt)}$ = 0.207 →
w_{max} = 141.9
← $m_{sw(opt)}$ = 0.068
0
0.05
0.1
0.15
0.2
0.25
m_{sw} [kg_{sw}/kg_{exh}]
(b)

Figure 13